IEEE Access
Multidisciplinary ⋮ Rapid Review ⋮ Open Access Journal

Received July 30, 2018, accepted September 19, 2018, date of publication September 28, 2018, date of current version October 25, 2018.

Digital Object Identifier 10.1109/ACCESS.2018.2872745

Finite-Time Projective Synchronization of Memristor-Based BAM Neural Networks and Applications in Image Encryption

WEIPING WANG[1,2,3,4], XIAO WANG[1], XIONG LUO[1,2] (Member, IEEE), AND MANMAN YUAN[1]

[1]School of Computer and Communication Engineering, University of Science and Technology Beijing, Beijing 100083, China
[2]Beijing Key Laboratory of Knowledge Engineering for Materials Science, Beijing 100083, China
[3]Institute of Physics, Humboldt-University, 10099 Berlin, Germany
[4]Potsdam Institute for Climate Impact Research, 14412 Potsdam, Germany

Corresponding author: Weiping Wang (weipingwangjt@ustb.edu.cn) and Xiao Wang (xavier_wangxiao@163.com)

This work was supported in part by the National Key Research and Development Program of China under Grant 2017YFB0702300, in part by the State Scholarship Fund of China Scholarship Council (CSC), in part by the National Natural Science Foundation of China under Grant 61603032 and Grant 61174103, in part by the Fundamental Research Funds for the Central Universities under Grant 06500025, in part by the National Key Technologies R&D Program of China under Grant 2015BAK38B01, and in part by the University of Science and Technology Beijing–National Taipei University of Technology Joint Research Program under Grant TW201705.

ABSTRACT Inspired by security applications in the image transmission, this paper focuses on the usage of chaotic properties of memristor-based bidirectional associate memory neural networks (MBAMNNs) for image encryption against illegal attack. A class of memristor-based bidirectional associate memory neural networks with delays and stochastic perturbations is formulated and analyzed. Based on drive-response concept, Itô's differential formula and inequality technique, some sufficient criteria are obtained to guarantee the finite-time projective synchronization. In order to realize the image encryption, we propose a chaotic color image encryption algorithm based on MBAMNNs. Illustrative examples are provided to verify the developed finite-time projective synchronization results. And we also show the great chaotic properties of the models proposed in this paper. Analysis of the encryption effect demonstrated the security of the proposed image encryption algorithm, and the potential applications of our models in secure image transmission are analyzed.

INDEX TERMS Finite-time projective synchronization, image encryption, memristor-based BAM neural networks, stochastic perturbation.

I. INTRODUCTION

During the past few decades, image encryption has attracted much attention from worldwide researchers due to its important applications in secure image transmission [1]–[4]. However, transmission of encrypted large images performs inefficiently by means of traditional image encryption schemes. To overcome the drawbacks of traditional encryption algorithms, chaotic encryption algorithm was proposed [5]. Chaotic image encryption algorithm provides a fast and secure way for image transmission, which is based on the chaotic systems.

Chaotic systems have many useful properties such as the sensitivity to their initial values and system parameters, pseudo-randomness, ergodicity, etc.. Quality of properties of chaotic systems determines the effectiveness of chaotic image encryption. Weak chaotic properties may lead to the problems of small key space and low security. Therefore, various chaotic systems with great chaotic properties are designed and widely used to generate the pseudo-random keystreams for chaotic image encryption [6]–[10]. In [6], authors presented a new chaotic system by combining Logistic, Sine and Tent systems. A new two-dimensional hyperchaotic map was proposed in [10]. Recently, memristor-based BAM neural networks is considered in chaotic image encryption due to its hyperchaotic properties.

Memristor-based BAM neural networks is a form of BAM neural networks [11]. This form of BAM neural networks is built replacing resistors with memristors. Memristor is a nonlinear circuit element with memory function. Superior non-volatile characteristic of memristor promotes the chaotic properties of memristive BAM neural networks. Memristor-based BAM neural networks consists of two layers of neurons. Neurons in one layer are completely connected to neurons in the other layer, while neurons in the same layer are not interconnected [12]. The structure of two layers gives memristor-based BAM neural networks powerful associative memory capabilities and hyperchaotic properties. Hence, it is interesting and significant to investigate the dynamic behaviors of memristor-based BAM neural networks [13], [14] and its applications in chaotic image encryption and secure image transmission. For instance, authors in [13] were concerned with anti-synchronization results for a class of memristor-based BAM neural networks with different memductance functions and time-varying delays.

Secure image transmission is based on the synchronization control between drive systems and response systems. L.M. Pecora and T.L. Carroll introduced the synchronization in chaotic system [15]. Veljko Milanović investiagted the synchronization of chaotic neural networks for secure communications in 1996 [16]. Recently, efforts have been devoted to the synchronization control of memristor-based neural networks [17]–[19], especially memristor-based BAM neural networks [20]–[23]. However, most studies of synchronization are about infinite-time synchronization control. Infinite-time synchronization can not determine the time for reaching complete synchronization, which may cause the inconsistency between the sent time and the receipt time. The inconsistency caused by infinite-time synchronization control is often undesirable in practical applications. Therefore, the study of the synchronization that can be reached in finite time is important [24]–[29]. Furthermore, projective synchronization can strengthen the security of image transmission and it is widely employed in secure communication [30]–[32]. In [33]–[36], authors studied the projective synchronization of memristor-based neural networks, and authors in [36] investigate the projective synchronization of BAM neural networks. Authors investigated the fixed-time synchronization of memristor-based BAM neural networks with discrete delay in [37]. As far as we know, few scholars have studied the finite-time projective synchronization of memristor-based BAM neural networks with time delays and stochastic perturbations, so in this paper we will fill this gap.

Inspired by the above discussions, this paper investigates the problem of finite-time projective synchronization of MBAMNNs with time delays and stochastic perturbations and then we applicate it in chaotic image encryption. The main contributions of this paper lie in the following aspects:

1) We propose two memristor-based BAM neural networks models. Since these models have great chaotic properties, they can be employed in image encryption algorithm effectively.
2) We consider the stochastic perturbations and time delays in our models and we get some corresponding criteria for finite-time projective synchronization of memristor-based BAM neural networks. These criteria can be applied to guarantee the secure image transmission.
3) An image encryption algorithm is also designed based on the memristor-based BAM neural networks models that we will propose in this paper.

The rest of this paper is organized as follows. In Section 2, we describe models of drive-response system. Inspired by [37], we introduce some necessary preliminaries. In Section 2, two feedback controllers are designed and conditions of finite-time projective synchronization of MBAMNNs are presented. In Section 4, four examples are provided to demonstrate the validity of proposed results and show the image encryption applications. Section 5 draws the conclusion.

II. MODEL DESCRIPTION AND PRELIMINARIES

In this paper, we consider the following memristor-based BAM neural networks with time delays.

$$\begin{cases} dx_i(t) = [-\delta_i(x_i(t))x_i(t) + \sum_{j=1}^{m} a_{ji}(x_i(t))f_j(y_j(t)) \\ \qquad + \sum_{j=1}^{m} b_{ji}(x_i(t))f_j(y_j(t-\tau(t)))]dt, \\ dy_j(t) = [-\rho_i(y_j(t))y_j(t) + \sum_{i=1}^{n} c_{ij}(y_j(t))g_j(x_j(t)) \\ \qquad + \sum_{i=1}^{n} d_{ij}(y_j(t))g_j(x_j(t-\tau(t)))]dt, \end{cases} \tag{1}$$

where $t \geq 0$, $i = 1, 2, ..., n$, $j = 1, 2, ..., m$; $x_i(t)$ and $y_j(t)$ donate the voltage of the capacitors $\mathcal{C}_i$ and $\hat{\mathcal{C}}_j$ of the i-th neuron in x-layer and j-th in y-layer, respectively; $\delta_i > 0$ and $\rho_j > 0$ represent the rates of neuron self-inhibition; $f_j(\cdot)$ and $g_i(\cdot)$ are the neuron activation functions; $\tau(t)$ is the time-varying delay and satisfies $0 \leq \tau(t) \leq \theta$, $\dot{\tau}(t) \leq \tau$; $a_{ji}, b_{ji}, c_{ij}, d_{ij}$ are connection weights, which are given by

$$\delta_i(\gamma) = \begin{cases} \acute{\delta}_i, & |\gamma| < T_i, \\ \grave{\delta}_i, & |\gamma| > T_i, \end{cases} \quad \rho_j(\gamma) = \begin{cases} \acute{\rho}_j, & |\gamma| < \hat{T}_j, \\ \grave{\rho}_j, & |\gamma| > \hat{T}_j, \end{cases}$$

$$a_{ji}(\gamma) = \begin{cases} \acute{a}_{ji}, & |\gamma| < T_i, \\ \grave{a}_{ji}, & |\gamma| > T_i, \end{cases} \quad c_{ij}(\gamma) = \begin{cases} \acute{c}_{ij}, & |\gamma| < \hat{T}_j, \\ \grave{c}_{ij}, & |\gamma| > \hat{T}_j, \end{cases}$$

$$b_{ji}(\gamma) = \begin{cases} \acute{b}_{ji}, & |\gamma| < T_i, \\ \grave{b}_{ji}, & |\gamma| > T_i, \end{cases} \quad d_{ij}(\gamma) = \begin{cases} \acute{d}_{ij}, & |\gamma| < \hat{T}_j, \\ \grave{d}_{ij}, & |\gamma| > \hat{T}_j, \end{cases}$$

where the switching jumps T_i, $\hat{T}_j$ are positive constants, while $\acute{\delta}_i$, $\grave{\delta}_i$, $\acute{\rho}_j$, $\grave{\rho}_j$, $\acute{a}_{ji}$, $\grave{a}_{ji}$, $\acute{b}_{ji}$, $\grave{b}_{ji}$, $\acute{c}_{ij}$, $\grave{c}_{ij}$, $\acute{d}_{ij}$, $\grave{d}_{ij}$ are constants. The initial values of system (1) are assumed to be $x(s) = \psi(s) \in \mathcal{C}([-\tau, 0], \mathbb{R}^n)$ and $y(s) = \phi(s) \in \mathcal{C}([-\tau, 0], \mathbb{R}^m)$.

Since the drive-response concept is used to derive the criteria of finite-time projective synchronization and system (1) is regarded as the drive system, the corresponding response system is presented as follows

$$\begin{cases} d\tilde{x}_i(t) = [-\delta_i(\tilde{x}_i(t))\tilde{x}_i(t) + \sum_{j=1}^{m} a_{ji}(\tilde{x}_i(t))f_j(\tilde{y}_j(t)) \\ \qquad + \sum_{j=1}^{m} b_{ji}(\tilde{x}_i(t))f_j(\tilde{y}_j(t-\tau(t))) + u_i(t)]dt, \\ d\tilde{y}_j(t) = [-\rho_i(\tilde{y}_j(t))\tilde{y}_j(t) + \sum_{i=1}^{n} c_{ij}(\tilde{y}_j(t))g_j(\tilde{x}_j(t)) \\ \qquad + \sum_{i=1}^{n} d_{ij}(\tilde{y}_j(t))g_j(\tilde{x}_j(t-\tau(t))) + v_j(t)]dt, \end{cases} \tag{2}$$

where $i = 1, 2, ..., n$, $j = 1, 2, ..., m$; $u_i(t)$ and $v_j(t)$ are the feedback controllers to be designed.

In consideration of stochastic perturbations, the corresponding response system is described as follows

$$\begin{cases} d\tilde{x}_i(t) = [-\delta_i(\tilde{x}_i(t))\tilde{x}_i(t) + \sum_{j=1}^{m} a_{ji}(\tilde{x}_i(t))f_j(\tilde{y}_j(t)) \\ \qquad + \sum_{j=1}^{m} b_{ji}(\tilde{x}_i(t))f_j(\tilde{y}_j(t-\tau(t))) + u_i(t)]dt \\ \qquad + \sum_{j=1}^{m} \sigma_{ji}(t, e_j^y(t), e_j^y(t-\tau(t))d\omega_j(t), \\ d\tilde{y}_j(t) = [-\rho_i(\tilde{y}_j(t))\tilde{y}_j(t) + \sum_{i=1}^{n} c_{ij}(\tilde{y}_j(t))g_j(\tilde{x}_j(t)) \\ \qquad + \sum_{i=1}^{n} d_{ij}(\tilde{y}_j(t))g_j(\tilde{x}_j(t-\tau(t))) + v_j(t)]dt \\ \qquad + \sum_{i=1}^{n} \tilde{\sigma}_{ij}(t, e_i^x(t), e_i^x(t-\tau(t))d\tilde{\omega}_i(t), \end{cases} \tag{3}$$

where $i = 1, 2, ..., n$, $j = 1, 2, ..., m$; $\tilde{\omega}_i$ and $\omega_j(t)$ are n-dimensional and m-dimensional Brownian motion defined on a complete probability space $(\Omega, \mathcal{F}, \mathcal{P})$ with a natural filtration $\{\mathcal{F}_t\}_{t\geq 0}$. $\sigma_{ji}(\cdot)$ and $\tilde{\sigma}_{ij}(\cdot)$ are the noise intensity function matrices, where $i = 1, 2, ..., n$ and $j = 1, 2, ..., m$. Assume the initial values of system (2) is the same as (3), which are $\tilde{x}(s) = \tilde{\psi}(s) \in \mathcal{C}([-\tau, 0], \mathbb{R}^n)$ and $\tilde{y}(s) = \tilde{\phi}(s) \in \mathcal{C}([-\tau, 0], \mathbb{R}^m)$.

The errors of projective synchronization is set as follows

$$\begin{cases} e_i^x(t) = \tilde{x}_i(t) - \alpha_i(t)x_i(t), \\ e_j^y(t) = \tilde{y}_j(t) - \beta_i(t)y_j(t), \end{cases} \tag{4}$$

where $i = 1, 2, ..., n$, $j = 1, 2, ..., m$; $\alpha(t)$ and $\beta(t)$ are bounded and differentiable scalars with $|\alpha(t)| < \xi$, $|\beta(t)| < \eta$, where ξ and η are positive constants.

In order to obtain the criteria of finite-time projective synchronization, we need the following assumptions.

Assumption 1: There exists constant $p_j > 0$, such that $|f_j(\cdot)| \leq p_j$, where $j = 1, 2, ..., m$.

Assumption 2: There exists constant $q_i > 0$, such that $|g_i(\cdot)| \leq q_i$, where $i = 1, 2, ..., n$.

Assumption 3: There exist two real matrices $G_1 = diag(g_{11}, g_{12}, ..., g_{1n}) \geq 0$ and $G_2 = diag(g_{21}, g_{22}, ..., g_{2n}) \geq 0$, such that

$$trace[\sigma^T(t, x, y)\sigma(t, x, y)] \leq x^T(t)G_1x(t) + y^T(t)G_2y(t).$$

Assumption 4: There exist two real matrices $H_1 = diag(h_{11}, h_{12}, ..., h_{1n}) \geq 0$ and $H_2 = diag(h_{21}, h_{22}, ..., h_{2n}) \geq 0$, such that

$$trace[\tilde{\sigma}^T(t, x, y)\tilde{\sigma}(t, x, y)] \leq x^T(t)H_1x(t) + y^T(t)H_2y(t).$$

Lemma 1:

$$\begin{aligned} &sign(e_i^x(t))(-\delta_i(\tilde{x}_i(t))\tilde{x}_i(t) + \alpha_i(t)\delta_i(x_i(t))x_i(t)) \\ &\quad \leq -\min\{\delta_i\}\left|e_i^x\right| + (1 + \left|\xi_i - 1\right|)\left|\grave{\delta}_i - \acute{\delta}_i\right|T_i, \\ &\quad for\ i = 1, 2, ..., n. \end{aligned}$$

Proof: Here we discuss four cases.

(1) When $|\tilde{x}_i(t)| < T_i$ and $|x_i(t)| < T_i$,

$$\begin{aligned} &sign(e_i^x(t))(-\delta_i(\tilde{x}_i(t))\tilde{x}_i(t) + \alpha_i(t)\delta_i(x_i(t))x_i(t)) \\ &\quad = sign(e_i^x(t))(-\acute{\delta}_i\tilde{x}_i(t) + \alpha_i(t)\acute{\delta}_ix_i(t)) \\ &\quad = -sign(e_i^x(t))\left[\acute{\delta}_i(\tilde{x}_i(t) - \alpha_i(t)x_i(t))\right] \\ &\quad = -\acute{\delta}_i\left|e_i^x\right| \leq -\min\{\delta_i\}\left|e_i^x\right|; \end{aligned}$$

(2) When $|\tilde{x}_i(t)| > T_i$ and $|x_i(t)| > T_i$,

$$\begin{aligned} &sign(e_i^x(t))(-\delta_i(\tilde{x}_i(t))\tilde{x}_i(t) + \alpha_i(t)\delta_i(x_i(t))x_i(t)) \\ &\quad = sign(e_i^x(t))(-\grave{\delta}_i\tilde{x}_i(t) + \alpha_i(t)\grave{\delta}_ix_i(t)) \\ &\quad = -\grave{\delta}_i\left|e_i^x\right| \leq -\min\{\delta_i\}\left|e_i^x\right|; \end{aligned}$$

(3) When $|\tilde{x}_i(t)| < T_i$ and $|x_i(t)| > T_i$,

$$\begin{aligned} &sign(e_i^x(t))(-\delta_i(\tilde{x}_i(t))\tilde{x}_i(t) + \alpha_i(t)\delta_i(x_i(t))x_i(t)) \\ &\quad = sign(e_i^x(t))(-\acute{\delta}_i\tilde{x}_i(t) + \alpha_i(t)\grave{\delta}_ix_i(t)) \\ &\quad = sign(e_i^x(t))(-\acute{\delta}_i\tilde{x}_i(t) + \grave{\delta}_i\tilde{x}_i(t) - \grave{\delta}_i\tilde{x}_i(t) \\ &\qquad + \alpha_i(t)\grave{\delta}_ix_i(t)) \\ &\quad = sign(e_i^x(t))(\grave{\delta}_i - \acute{\delta}_i)\tilde{x}_i(t) - \grave{\delta}_i\left|e_i^x\right| \\ &\quad \leq -\min\{\delta_i\}\left|e_i^x\right| + \left|\grave{\delta}_i - \acute{\delta}_i\right|T_i; \end{aligned}$$

(4) When $|\tilde{x}_i(t)| > T_i$ and $|x_i(t)| < T_i$,

$$\begin{aligned} &sign(e_i^x(t))(-\delta_i(\tilde{x}_i(t))\tilde{x}_i(t) + \alpha_i(t)\delta_i(x_i(t))x_i(t)) \\ &\quad = sign(e_i^x(t))(-\grave{\delta}_i\tilde{x}_i(t) + \alpha_i(t)\acute{\delta}_ix_i(t)) \\ &\quad = sign(e_i^x(t))(-\grave{\delta}_i\tilde{x}_i(t) + \alpha_i(t)\acute{\delta}_ix_i(t) + \alpha_i(t)\grave{\delta}_ix_i(t) \\ &\qquad - \alpha_i(t)\grave{\delta}_ix_i(t)) \\ &\quad = sign(e_i^x(t))\alpha_i(t)(\grave{\delta}_i - \acute{\delta}_i)x_i(t) - \grave{\delta}_i\left|e_i^x\right| \\ &\quad \leq -\min\{\delta_i\}\left|e_i^x\right| + \alpha_i(t)\left|\grave{\delta}_i - \acute{\delta}_i\right|T_i \\ &\quad \leq -\min\{\delta_i\}\left|e_i^x\right| + (1 + |\xi_i - 1|)\left|\grave{\delta}_i - \acute{\delta}_i\right|T_i. \end{aligned}$$

The proof is completed. □

Lemma 2:

$$\begin{aligned} &sign(e_j^y(t))(-\rho_j(\tilde{y}_j(t))\tilde{y}_j(t) + \beta_j(t)\rho_j(y_j(t))y_j(t)) \\ &\quad \leq -\min\{\rho_j\}\left|e_j^y\right| + (1 + \left|\eta_j - 1\right|)\left|\grave{\rho}_j - \acute{\rho}_j\right|\hat{T}_j, \\ &\quad for\ j = 1, 2, ..., m. \end{aligned}$$

Similar to the proof of Lemma 1, here we omit it. □

Lemma 3:

$$\Big|\sum_{j=1}^{m} a_{ji}(\tilde{x}_i(t))f_j(\tilde{y}_j(t)) + \sum_{j=1}^{m} b_{ji}(\tilde{x}_i(t))f_j(\tilde{y}_j(t-\tau(t))) - \sum_{j=1}^{m}\alpha_i(t)a_{ji}(x_i(t))f_j(y_j(t)) - \sum_{j=1}^{m}\alpha_i(t)b_{ji}(x_i(t))f_j(y_j(t-\tau(t)))\Big| \le \sum_{j=1}^{m}\left[(\max\{|a_{ji}|\} + \max\{|b_{ji}|\})(1+\xi_i)p_j\right],$$
$$\textit{for } i = 1, 2, \ldots, n.$$

Proof: Here we discuss four cases. (1) When $|\tilde{x}_i(t)| < T_i$ and $|x_i(t)| < T_i$,

$$\begin{aligned}
&\Big|\sum_{j=1}^{m}\{\acute{a}_{ji}[f_j(\tilde{y}_j(t)) - \alpha_i(t)f_j(y_j(t))] + \acute{b}_{ji}[f_j(\tilde{y}_j(t-\tau(t))) - \alpha_i(t)f_j(y_j(t-\tau(t)))]\}\Big|\\
&\le \sum_{j=1}^{m}\Big[|\acute{a}_{ji}f_j(\tilde{y}_j(t)) - \alpha_i(t)f_j(y_j(t))| + |\acute{b}_{ji}f_j(\tilde{y}_j(t-\tau(t))) - \alpha_i(t)f_j(y_j(t-\tau(t)))|\Big]\\
&\le \sum_{j=1}^{m}\{|\acute{a}_{ji}|\left[|f_j(\tilde{y}_j(t))| + |\alpha_i(t)f_j(y_j(t))|\right] + |\acute{b}_{ji}|\left[|f_j(\tilde{y}_j(t-\tau(t)))| + |\alpha_i(t)f_j(y_j(t-\tau(t)))|\right]\}\\
&\le \sum_{j=1}^{m}\left\{|\acute{a}_{ji}|(p_j+\xi_i p_j) + |\acute{b}_{ji}|(p_j+\xi_i p_j)\right\}\\
&\le \sum_{j=1}^{m}\left[(\max\{|a_{ji}|\} + \max\{|b_{ji}|\})(1+\xi_i)p_j\right];
\end{aligned}$$

(2) When $|\tilde{x}_i(t)| > T_i$ and $|x_i(t)| > T_i$,

$$\begin{aligned}
&\Big|\sum_{j=1}^{m}\{\grave{a}_{ji}[f_j(\tilde{y}_j(t)) - \alpha_i(t)f_j(y_j(t))] + \grave{b}_{ji}[f_j(\tilde{y}_j(t-\tau(t))) - \alpha_i(t)f_j(y_j(t-\tau(t)))]\}\Big|\\
&\le \sum_{j=1}^{m}\left[(\max\{|a_{ji}|\} + \max\{|b_{ji}|\})(1+\xi_i)p_j\right];
\end{aligned}$$

(3) When $|\tilde{x}_i(t)| < T_i$ and $|x_i(t)| > T_i$,

$$\begin{aligned}
&\Big|\sum_{j=1}^{m}\Big[\acute{a}_{ji}f_j(\tilde{y}_j(t)) - \alpha_i(t)\grave{a}_{ji}f_j(y_j(t)) + \acute{b}_{ji}f_j(\tilde{y}_j(t-\tau(t))) - \alpha_i(t)\grave{b}_{ji}f_j(y_j(t-\tau(t)))\Big]\Big|\\
&\le \sum_{j=1}^{m}\Big[|\acute{a}_{ji}f_j(\tilde{y}_j(t))| + |\grave{a}_{ji}\alpha_i(t)f_j(y_j(t))| + |\acute{b}_{ji}f_j(\tilde{y}_j(t-\tau(t)))| + |\grave{b}_{ji}\alpha_i(t)f_j(y_j(t-\tau(t)))|\Big]\\
&\le \sum_{j=1}^{m}\left(|\acute{a}_{ji}|p_j + |\grave{a}_{ji}|\xi_i p_j + |\acute{b}_{ji}|p_j + |\grave{b}_{ji}|\xi_i p_j\right)\\
&\le \sum_{j=1}^{m}\Big[(\max\{|a_{ji}|\} + \max\{|b_{ji}|\})(1+\xi_i)p_j\Big];
\end{aligned}$$

(4) When $|\tilde{x}_i(t)| > T_i$ and $|x_i(t)| < T_i$,

$$\begin{aligned}
&\Big|\sum_{j=1}^{m}\Big[\grave{a}_{ji}f_j(\tilde{y}_j(t)) - \alpha_i(t)\acute{a}_{ji}f_j(y_j(t)) + \grave{b}_{ji}f_j(\tilde{y}_j(t-\tau(t))) - \alpha_i(t)\acute{b}_{ji}f_j(y_j(t-\tau(t)))\Big]\Big|\\
&\le \sum_{j=1}^{m}\left[(\max\{|a_{ji}|\} + \max\{|b_{ji}|\})(1+\xi_i)p_j\right].
\end{aligned}$$

The proof is completed. □

Lemma 4:

$$\Big|\sum_{i=1}^{n} c_{ij}(\tilde{y}_j(t))g_i(\tilde{x}_i(t)) + \sum_{i=1}^{n} d_{ij}(\tilde{y}_j(t))g_i(\tilde{x}_i(t-\tau(t))) - \sum_{i=1}^{n}\beta_i(t)c_{ij}(y_j(t))g_i(x_i(t)) - \sum_{i=1}^{n}\beta_i(t)d_{ij}(y_j(t))g_i(x_i(t-\tau(t)))\Big| \le \sum_{i=1}^{n}\left[(\max\{|c_{ij}|\} + \max\{|d_{ij}|\})(1+\eta_j)q_i\right],$$
$$\textit{for } j = 1, 2, \ldots, m.$$

Similar to the proof of Lemma 3, here we omit it. □

Lemma 5 (Mao [38]): Assume the error system exists a unique solution $e(t,\psi)$ on $t > 0$ for any given initial data $\{x(\theta) : -\tau \le \theta \le 0\} = \psi \in \mathcal{C}_F^b([-\tau, 0]; \mathbb{R}^n)$, moreover, both $f(x, y, t)$ and $g(x, y, t)$ are locally bounded in (x, y) and uniformly bounded in t, where $(x, y, t) \in \mathbb{R}^n \times \mathbb{R}^n \times \mathbb{R}_+$. If there are a function $V \in \mathcal{C}^{2,1}(\mathbb{R}^n \times \mathbb{R}_+; \mathbb{R}_+)$, $\beta \in L^1(\mathbb{R}_+, \mathbb{R}_+)$ and $\omega_1, \omega_2 \in \mathcal{C}(\mathbb{R}^n; \mathbb{R}_+)$ such that

$$\begin{aligned}
\mathcal{L}V(x, y, t) &\le \beta(t) - \omega_1(x) + \omega_y(y),\\
\omega_1(x) &> \omega_2(x),\ x \in \mathbb{R}^n,\\
\lim_{\|x\|\to\infty}\inf_{0\le t\le\infty} V(x, t) &= \infty. \qquad (5)
\end{aligned}$$

Then

$$\lim_{t\to+\infty} x(t,\psi) = 0 \quad a.s. \qquad (6)$$

for every $\psi \in \mathcal{C}_F^b([-\tau, 0]; \mathbb{R}^n)$.

Lemma 6 (Hardy, Littlewood, & Polya, 1952 [39]): If $x_i \ge 0$ and $0 < p \le 1$ where $i = 1, 2, \ldots, n$, then we have

$$\sum_{i=1}^{n} x_i^p \ge \left(\sum_{i=1}^{n} x_i\right)^p.$$

Definition 1: The drive system (1) is said to achieve finite-time projective synchronization with the response system (2) if there exists a constant $t_1(e(0)) \geq 0$ satisfies

$$\begin{cases} \lim_{t\to t_1(e(0))} ||e_i^x(t)|| = \lim_{t\to t_1(e(0))} ||\tilde{x}_i(t) - \alpha_i(t)x_i(t))|| = 0, \\ \lim_{t\to t_1(e(0))} \| e_j^y(t)\| = \lim_{t\to t_1(e(0))} \| \tilde{y}_j(t) - \beta_j(t)y_j(t)\| = 0, \end{cases}$$

where $i = 1, 2, \ldots, n$ and $j = 1, 2, \ldots, m$; $t_1(e(0))$ is called the settling time that is depended on the initial value $e(0)$ and $e(t) = (e_1^x(t), e_2^x(t), \ldots, e_n^x(t), e_1^y(t), e_2^y(t), \ldots, e_m^y(t))^T$.

Lemma 7 (Tang, 1998 [40]): Assume that a continuous positive-definite function V(t) satisfies the following differential inequality:

$$\dot{V}(x(t)) \leq -kV^{\eta}(x(t)), \quad \forall t \geq t_0, \; V(t_0) \geq 0,$$

where $k > 0$, $0 < \mu < 1$ are two constants. Then, for any given t_0, V (t) satisfies the following inequality:

$$V^{1-\mu}(t) \leq V^{1-\mu}(t_0) - k(1-\mu)(t-t_0), \quad t_0 \leq t \leq t_1,$$

and

$$V(x(t)) \equiv 0, \quad \forall t \geq t_1,$$

Drive and response system can achieve synchronization in finite-time and the settling time t_1 is given by

$$t_1 = t_0 + \frac{V^{1-\mu}(x(t_0))}{k(1-\mu)}.$$

III. MAIN RESULTS

In this section, some criteria of the finite-time projective synchronization will be obtained.

Theorem 1: Assume the Assumptions 1 and 2 hold and the feedback controllers are designed as follows

$$\begin{cases} u_i(t) = -\lambda_{1i} sign(e_i^x(t)) - \lambda_{2i} e_i^x(t) \\ \qquad - \lambda_{3i} sign(e_i^x(t))|e_i^x(t)|^{\varkappa} \\ \qquad + sign(e_i^x(t))\dot{\alpha}_i(t)x_i(t), \\ v_j(t) = -l_{1j} sign(e_j^y(t)) - l_{2j} e_j^y(t) \\ \qquad - l_{3j} sign(e_j^y(t))|e_j^y(t)|^{\varkappa} \\ \qquad + sign(e_j^y(t))\dot{\beta}_j(t)y_j(t), \end{cases} \tag{7}$$

where $i = 1, 2, \ldots, n, j = 1, 2, \ldots, n$, $0 < \varkappa < 1$. λ_{1i}, λ_{2i}, λ_{3i}, l_{1j}, l_{2j}, l_{3j} are constants and satisfy

$$\begin{cases} \lambda_{1i} > \sum_{j=1}^{m} \left[(\max\{|a_{ji}|\} + \max\{|b_{ji}|\})(1+\xi_i)p_j \right] \\ \qquad + (1 + |\xi_i - 1|) \left| \grave{\delta}_i - \acute{\delta}_i \right| T_i, \\ l_{1j} > \sum_{i=1}^{n} \left[(\max\{|c_{ij}|\} + \max\{|d_{ij}|\})(1+\eta_j)q_i \right] \\ \qquad + (1 + |\eta_j - 1|) \left| \grave{\rho}_j - \acute{\rho}_j \right| \hat{T}_j, \\ \lambda_{2i} > -\min\{\delta_i\}, \\ l_{2j} > -\min\{\rho_j\}, \\ \lambda_{3i} > 0, \quad l_{3j} > 0, \end{cases} \tag{8}$$

then systems (1) and (2) can achieve the finite-time projective synchronization within $t_1 = \frac{V^{1-\frac{\varkappa+1}{2}}(0)}{2^{\frac{\varkappa+1}{2}}(min_{i,j}\{\lambda_{3i}, l_{3j}\})(1-\frac{\varkappa+1}{2})}$.

Proof: We consider the following Lyapunov-Krasovskii function

$$V(t) = V_1(t) + V_2(t),$$

where

$$V_1(t) = \frac{1}{2}\sum_{i=1}^{n}(e_i^x(t))^2, \quad V_2(t) = \frac{1}{2}\sum_{j=1}^{m}(e_j^y(t))^2.$$

The derivative of $V_1(t)$ can be calculated as

$$\begin{aligned} \dot{V}_1(t) = \sum_{i=1}^{n} e_i^x(t) \Big\{ &- \delta_i(\tilde{x}_i(t))\tilde{x}_i(t) \\ &+ \alpha_i(t)\delta_i(x_i(t))x_i(t) \\ &+ \sum_{j=1}^{m} a_{ji}(\tilde{x}_i(t))f_j(\tilde{y}_j(t)) \\ &- \sum_{j=1}^{m} \alpha_i(t)a_{ji}(x_i(t))f_j(y_j(t)) \\ &+ \sum_{j=1}^{m} b_{ji}(\tilde{x}_i(t))f_j(\tilde{y}_j(t-\tau(t))) \\ &- \sum_{j=1}^{m} \alpha_i(t)b_{ji}(x_i(t))f_j(y_j(t-\tau(t))) \\ &+ u_i(t) - \dot{\alpha}_i(t)x_i(t) \Big\}, \end{aligned}$$

Under Lemma 1 and 3, we get

$$\begin{aligned} \dot{V}_1(t) \leq \sum_{i=1}^{n} |e_i^x(t)| \Big\{ &- \min\{\delta_i\} \left| e_i^x \right| \\ &+ (1 + |\xi_i - 1|) \left| \grave{\delta}_i - \acute{\delta}_i \right| T_i \\ &+ sign(e_i^x(t)) \sum_{j=1}^{m} \Big[(\max\{|a_{ji}|\} \\ &+ \max\{|b_{ji}|\})(1+\xi_i)p_j \Big] \\ &+ sign(e_i^x(t))u_i(t) - sign(e_i^x(t))\dot{\alpha}_i(t)x_i(t) \Big\} \\ \leq \sum_{i=1}^{n} |e_i^x(t)| \Big\{ &- \min\{\delta_i\} \left| e_i^x \right| \\ &+ (1 + |\xi_i - 1|) \left| \grave{\delta}_i - \acute{\delta}_i \right| T_i \\ &+ sign(e_i^x(t)) \sum_{j=1}^{m} \Big[(\max\{|a_{ji}|\} \\ &+ \max\{|b_{ji}|\})(1+\xi_i)p_j \Big] \\ &- \lambda_{1i} - \lambda_{2i}|e_i^x(t)| - \lambda_{3i}|e_i^x(t)|^{\varkappa} \Big\}, \end{aligned}$$

then we have

$$\dot{V}_1(t) \leq \sum_{i=1}^{n}\Big\{-(\lambda_{2i}+\min\{\delta_i\})(e_i^x(t))^2 + \Big\{(1+|\xi_i-1|)\Big|\grave{\delta}_i-\acute{\delta}_i\Big|T_i-\lambda_{1i} + \sum_{j=1}^{m}\Big[(\max\{a_{ji}\}+\max\{b_{ji}\})(1 +\xi_i)p_j\Big]\Big\}|e_i^x|-\lambda_{3i}|e_i^x|^{\varkappa+1}\Big\}. \quad (9)$$

Similarly, the derivative of $V_2(t)$ can be calculated as follows:

$$\dot{V}_2(t) \leq \sum_{j=1}^{m}\Big\{-(l_{2i}+\min\{\rho_j\})(e_j^y(t))^2 + \Big\{(1+|\eta_j-1|)\,|\grave{\rho}_j-\acute{\rho}_j|\,\hat{T}_j-l_{1j} + \sum_{i=1}^{n}\Big[(\max\{c_{ij}\}+\max\{d_{ij}\})(1 +\eta_j)q_i\Big]\Big\}|e_j^y|-l_{3j}|e_j^y|^{\varkappa+1}\Big\}. \quad (10)$$

Now combining (9) and (10), we get

$$\begin{aligned}\dot{V}(t) &= \dot{V}_1(t)+\dot{V}_2(t)\\ &\leq \sum_{i=1}^{n}\Big\{-(\lambda_{2i}+\min\{\delta_i\})(e_i^x(t))^2 + \Big\{(1+|\xi_i-1|)\Big|\grave{\delta}_i-\acute{\delta}_i\Big|T_i-\lambda_{1i} + \sum_{j=1}^{m}\Big[(\max\{a_{ji}\}+\max\{b_{ji}\})(1 +\xi_i)p_j\Big]\Big\}|e_i^x|-\lambda_{3i}|e_i^x|^{\varkappa+1}\Big\}\\ &\quad + \sum_{j=1}^{m}\Big\{-(l_{2i}+\min\{\rho_j\})(e_j^y(t))^2 + \Big\{(1+|\eta_j-1|)\,|\grave{\rho}_j-\acute{\rho}_j|\,\hat{T}_j-l_{1j} + \sum_{i=1}^{n}\Big[(\max\{c_{ij}\}+\max\{d_{ij}\})(1 +\eta_j)q_i\Big]\Big\}|e_j^y|-l_{3j}|e_j^y|^{\varkappa+1}\Big\}. \end{aligned} \quad (11)$$

Substituting (8) into (11) and using Lemma 6, we obtain

$$\begin{aligned}\dot{V}(t) &\leq -\sum_{i=1}^{n}\lambda_{3i}|e_i^x|^{\varkappa+1}-\sum_{j=1}^{m}l_{3j}|e_j^y|^{\varkappa+1}\\ &\leq -2^{\frac{\varkappa+1}{2}}(min_{i,j}\{\lambda_{3i},\text{ł}_{3j}\})\Big(\sum_{i=1}^{n}(\frac{1}{2}e_i^x(t))^2 + \frac{1}{2}\sum_{j=1}^{m}(e_j^y(t))^2\Big)^{\frac{\varkappa+1}{2}}\\ &\leq -2^{\frac{\varkappa+1}{2}}(min_{i,j}\{\lambda_{3i},\text{ł}_{3j}\})(V_1(t)+V_2(t))^{\frac{\varkappa+1}{2}}.\end{aligned}$$

It is obviously that

$$\dot{V}(t) \leq -2^{\frac{\varkappa+1}{2}}(min\{\lambda_{3i},\text{ł}_{3j}\})(V(t))^{\frac{\varkappa+1}{2}}. \quad (12)$$

According to Definition 1 and Lemma 7, system (1) and (2) can achieve the finite-time projective synchronization under feedback controller (7). Furthermore, we can get $k = 2^{\frac{\varkappa+1}{2}}(min_{i,j}\{\lambda_{3i},\text{ł}_{3j}\})$, $\mu = \frac{\varkappa+1}{2}$ and the settling time $t_1 = \frac{V^{1-\frac{\varkappa+1}{2}}(0)}{2^{\frac{\varkappa+1}{2}}(min_{i,j}\{\lambda_{3i},\text{ł}_{3j}\})(1-\frac{\varkappa+1}{2})}$. □

Corollary 1: Change the scalars $\alpha_i(t)$, $\beta_j(t)$ from functions to positive constants satisfying $\alpha_i \leq \xi_i$ and $\beta_j \leq \eta_j$, respectively. System (1) and (2) can achieve the finite-time modified projective synchronization under the following feedback controller

$$\begin{cases} u_i(t) = -\lambda_{1i}sign(e_i^x(t))-\lambda_{2i}e_i^x(t) \\ \qquad -\lambda_{3i}sign(e_i^x(t))|e_i^x(t)|^{\varkappa}, \\ v_j(t) = -l_{1j}sign(e_j^y(t))-l_{2j}e_j^y(t) \\ \qquad -l_{3j}sign(e_j^y(t))|e_j^y(t)|^{\varkappa}, \end{cases} \quad (13)$$

where $i = 1, 2, \ldots, n$, $j = 1, 2, \ldots, n$, $0 < \varkappa < 1$. λ_{1i}, λ_{2i}, λ_{3i}, l_{1j}, l_{2j}, l_{3j} are positive constants defined in Theorem 1.

Theorem 2: Now we are in a position to introduce the stochastic perturbations to response system. Assume the Assumptions 1 – 4 hold, while the G_1, G_2 in Assumption 3 and H_1, H_2 in Assumption 4 are known matrices. System (1) and (3) can finte-timely projectively synchronized within settling time $t_1 = \frac{V^{1-\frac{\varkappa+1}{2}}(0)}{2^{\frac{\varkappa+1}{2}}(min_{i,j}\{\lambda_{3i},\lambda_{4i},\text{ł}_{3j},l_{4j}\})(1-\frac{\varkappa+1}{2})}$ under feedback controller designed as follows

$$\begin{cases} u_i(t) = -\lambda_{1i}sign(e_i^x(t))-\lambda_{2i}e_i^x(t) \\ \qquad -\lambda_{3i}sign(e_i^x(t))|e_i^x(t)|^{\varkappa} \\ \qquad -\lambda_{4i}\frac{sign(e_i^x(t))}{|e_i^x(t)|}\Big(\int_{t-\tau(t)}^{t}(e_i^x(s))^2ds\Big)^{\frac{\varkappa+1}{2}} \\ \qquad +sign(e_i^x(t))\dot{\alpha}_i(t)x_i(t), \\ v_j(t) = -l_{1j}sign(e_j^y(t))-l_{2j}e_j^y(t)-l_{2j}e_j^y(t) \\ \qquad -l_{3j}sign(e_j^y(t))|e_j^y(t)|^{\varkappa} \\ \qquad -l_{4j}\frac{sign(e_j^y(t))}{|e_j^y(t)|}\Big(\int_{t-\tau(t)}^{t}(e_j^y(s))^2ds\Big)^{\frac{\varkappa+1}{2}} \\ \qquad +sign(e_j^y(t))\dot{\beta}_j(t)y_j(t), \end{cases} \quad (14)$$

where $i = 1, 2, ..., n, j = 1, 2, ..., n$; $0 < \varkappa < 1$, λ_{1i}, λ_{2i}, λ_{3i}, λ_{4i}, l_{1j}, l_{2j}, l_{3j}, l_{4j} satisfy the conditions as

$$\begin{cases} \lambda_{1i} > (1+|\xi_i-1|)\left|\grave{\delta}_i-\acute{\delta}_i\right| T_i \\ \qquad + \sum_{j=1}^{m}\left[(\max\{|a_{ji}|\}+\max\{|b_{ji}|\})(1+\xi_i)p_j\right], \\ \lambda_{2i} > -\min\{\delta_i\}+\frac{h_{1i}}{2}+\dfrac{h_{2i}}{2(1-\tau)}, \\ \lambda_{3i} > 0, \quad \lambda_{4i} > 0, \\ l_{1j} > (1+|\eta_j-1|)\left|\grave{\rho}_j-\acute{\rho}_j\right| \hat{T}_j \\ \qquad + \sum_{i=1}^{n}\left[(\max\{|c_{ij}|\}+\max\{|d_{ij}|\})(1+\eta_j)q_i\right], \\ l_{2j} > -\min\{\rho_j\}+\dfrac{g_{1j}}{2}+\dfrac{g_{2j}}{2(1-\tau)}, \\ l_{3j} > 0, \quad l_{4j} > 0. \end{cases} \tag{15}$$

Proof: We consider the following Lyapunov-Krasovskii function

$$V(t) = V_1(t) + V_2(t),$$

where

$$V_1(t) = \frac{1}{2}\sum_{i=1}^{n}(e_i^x(t))^2 + \frac{1}{2}\int_{t-\tau(t)}^{t}(e^y(s))^T M e^y(s)ds,$$

$$V_2(t) = \frac{1}{2}\sum_{j=1}^{m}(e_j^y(t))^2 + \frac{1}{2}\int_{t-\tau(t)}^{t}(e^x(s))^T N e^x(s)ds,$$

$i = 1, 2, ..., n$, $j = 1, 2, ..., m$; $M = diag(m_1, m_2, ..., m_m)$ and $N = diag(n_1, n_2, ..., n_n)$ are positive matrices, in which $0 < n_i, m_j < 1$.

By Itô's differential formula, the stochastic derivative of $V_1(t)$ can be calculated as

$$\begin{aligned} &\mathcal{L}V_1(t) \\ &= \sum_{i=1}^{n} e_i^x(t)\Big(-\delta_i(\tilde{x}_i(t))\tilde{x}_i(t)+\alpha_i(t)\delta_i(x_i(t))x_i(t) \\ &\quad+\sum_{j=1}^{m} a_{ji}(\tilde{x}_i(t))f_j(\tilde{y}_j(t)) \\ &\quad-\sum_{j=1}^{m} \alpha_i(t)a_{ji}(x_i(t))f_j(y_j(t)) \\ &\quad+\sum_{j=1}^{m} b_{ji}(\tilde{x}_i(t))f_j(\tilde{y}_j(t-\tau(t))) \\ &\quad-\sum_{j=1}^{m} \alpha_i(t)b_{ji}(x_i(t))f_j(y_j(t-\tau(t))) \\ &\quad+u_i(t)-sign(e_i^x(t))\dot{\alpha}_i(t)x_i(t)\Big)+\frac{1}{2}(e^y(t))^T M e^y(t) \\ &\quad+\frac{1}{2}trace[\sigma^T(t, e^y(t), e^y(t-\tau))\sigma(t, e^y(t), e^y(t-\tau))] \\ &\quad-\frac{1-\dot{\tau}(t)}{2}(e^y(t-\tau(t)))^T M e^y(t-\tau(t)). \end{aligned}$$

Since Assumptions 3 and 4 hold, we have

$$\begin{aligned} \mathcal{L}V_1(t) \le &\sum_{i=1}^{n} e_i^x(t)\Big(-\delta_i(\tilde{x}_i(t))\tilde{x}_i(t)+\alpha_i(t)\delta_i(x_i(t))x_i(t) \\ &+\sum_{j=1}^{m} a_{ji}(\tilde{x}_i(t))f_j(\tilde{y}_j(t)) \\ &-\sum_{j=1}^{m} \alpha_i(t)a_{ji}(x_i(t))f_j(y_j(t)) \\ &+\sum_{j=1}^{m} b_{ji}(\tilde{x}_i(t))f_j(\tilde{y}_j(t-\tau(t))) \\ &-\sum_{j=1}^{m} \alpha_i(t)b_{ji}(x_i(t))f_j(y_j(t-\tau(t))) \\ &+u_i(t)-sign(e_i^x(t))\dot{\alpha}_i(t)x_i(t)\Big) \\ &+\frac{1}{2}(e^y(t-\tau(t)))^T G_2 e^y(t-\tau(t)) \\ &-\frac{1-\tau}{2}(e^y(t-\tau(t)))^T M e^y(t-\tau(t)) \\ &+\frac{1}{2}(e^y(t))^T G_1 e^y(t)+\frac{1}{2}(e^y(t))^T M e^y(t). \end{aligned}$$

Now using the Lemma 1 and Lemma 3, we get

$$\begin{aligned} \mathcal{L}V_1(t) \le &\sum_{i=1}^{n} |e_i^x(t)|\Big\{-\min\{\delta_i\}\left|e_i^x\right| \\ &+(1+|\xi_i-1|)\left|\grave{\delta}_i-\acute{\delta}_i\right| T_i \\ &+sign(e_i^x(t))\sum_{j=1}^{m}\Big[(\max\{|a_{ji}|\} \\ &+\max\{|b_{ji}|\})(1+\xi_i)p_j\Big]+sign(e_i^x)u_i(t) \\ &-sign(e_i^x(t))\dot{\alpha}_i(t)x_i(t)\Big\} \\ &+\frac{1}{2}(e^y(t))^T(G_1+M)e^y(t) \\ &+\frac{1}{2}(e^y(t-\tau(t)))^T(G_2-(1-\tau)M)e^y(t-\tau(t)). \end{aligned}$$

According to the controller (14), it follows that

$$\begin{aligned} \mathcal{L}V_1(t) \le &\sum_{i=1}^{n} |e_i^x(t)|\Big\{-\min\{\delta_i\}\left|e_i^x\right| \\ &+(1+|\xi_i-1|)\left|\grave{\delta}_i-\acute{\delta}_i\right| T_i \\ &+sign(e_i^x(t))\sum_{j=1}^{m}\Big[(\max\{|a_{ji}|\} \\ &+\max\{|b_{ji}|\})(1+\xi_i)p_j\Big] \\ &-\lambda_{1i}-\lambda_{2i}|e_i^x(t)|-\lambda_{3i}|e_i^x(t)|^{\varkappa} \\ &-\lambda_{4i}\frac{|e_i^x(t)|}{|e_i^x(t)|}\Big(\int_{t-\tau(t)}^{t}(e_i^x(s))^2 ds\Big)^{\frac{\varkappa+1}{2}}\Big\} \end{aligned}$$

$$
\begin{aligned}
&+\frac{1}{2}(e^y(t))^T(G_1+M)e^y(t)\\
&+\frac{1}{2}(e^y(t-\tau(t)))^T(G_2-(1-\tau)M)e^y(t-\tau(t))\\
\le&\sum_{i=1}^{n}\Big\{-(\lambda_{2i}+\min\{\delta_i\})(e_i^x(t))^2\\
&-\lambda_{3i}|e_i^x(t)|^{\varkappa+1}-\lambda_{4i}(\int_{t-\tau(t)}^{t}n_i(e_i^x(s))^2ds)^{\frac{\varkappa+1}{2}}\\
&+\Big\{(1+|\xi_i-1|)\left|\grave{\delta}_i-\acute{\delta}_i\right|T_i\\
&+\sum_{j=1}^{m}\Big[(\max\{a_{ji}\}+\max\{b_{ji}\})(1+\xi_i)p_j\Big]\\
&-\lambda_{1i}\Big\}|e_i^x|\Big\}+\frac{1}{2}(e^y(t))^T(G_1+M)e^y(t)\\
&+\frac{1}{2}(e^y(t-\tau(t)))^T(G_2-(1-\tau)M)e^y(t-\tau(t)).
\end{aligned}\tag{16}
$$

Similarly, the stochastic derivative of $V_2(t)$ can be calculated as follows

$$
\begin{aligned}
\mathcal{L}V_2(t)=&\sum_{j=1}^{m}e_j^y(t)\Big(-\rho_j(\tilde{y}_j(t))\tilde{y}_j(t)+\beta_j(t)\rho_j(y_j(t))y_j(t)\\
&+\sum_{i=1}^{n}c_{ij}(\tilde{y}_j(t))g_i(\tilde{x}_i(t))\\
&-\sum_{i=1}^{n}\beta_j(t)c_{ij}(y_j(t))g_i(x_i(t))\\
&+\sum_{i=1}^{n}d_{ij}(\tilde{y}_j(t))g_i(\tilde{x}_i(t-\tau(t)))\\
&-\sum_{i=1}^{n}\beta_j(t)d_{ij}(y_j(t))g_i(x_i(t-\tau(t)))\\
&+v_j(t)-sign(e_j^y(t))\dot{\beta}_j(t)y_j(t)\Big)\\
&+\frac{1}{2}(e^x(t))^TNe^x(t)\\
&+\frac{1}{2}trace[\tilde{\sigma}^T(t,e^x(t),e^x(t\\
&-\tau))\tilde{\sigma}(t,e^x(t),e^x(t-\tau))]\\
&-\frac{1-\dot{\tau}(t)}{2}(e^x(t-\tau(t)))^TNe^x(t-\tau(t)).
\end{aligned}
$$

Under Lemma 2 and Lemma 4, we have

$$
\begin{aligned}
\mathcal{L}V_2(t)\le&\sum_{j=1}^{n}\{-(l_{2j}+\min\{\rho_j\})(e_j^y(t))^2\\
&-l_{3j}|e_j^y(t)|^{\varkappa+1}\\
&-l_{4j}(\int_{t-\tau(t)}^{t}m_j(e_j^y(s))^2ds)^{\frac{\varkappa+1}{2}}\\
&+\{(1+|\eta_j-1|)\left|\grave{\rho}_j-\acute{\rho}_j\right|\hat{T}_j\\
&+\sum_{i=1}^{n}\Big[(\max\{c_{ij}\}+\max\{d_{ij}\})(1\\
&+\eta_j)q_i\Big]-l_{1j}\}|e_j^y|\}\\
&+\frac{1}{2}(e^x(t))^T(H_1+N)e^x(t)\\
&+\frac{1}{2}(e^x(t-\tau(t)))^T(H_2\\
&-(1-\tau)N)e^x(t-\tau(t)).
\end{aligned}\tag{17}
$$

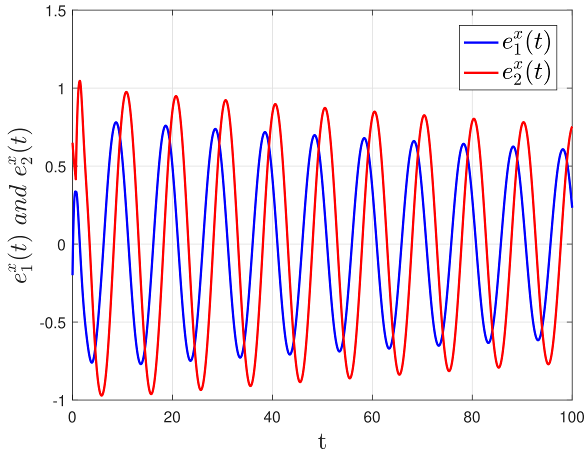

(a)

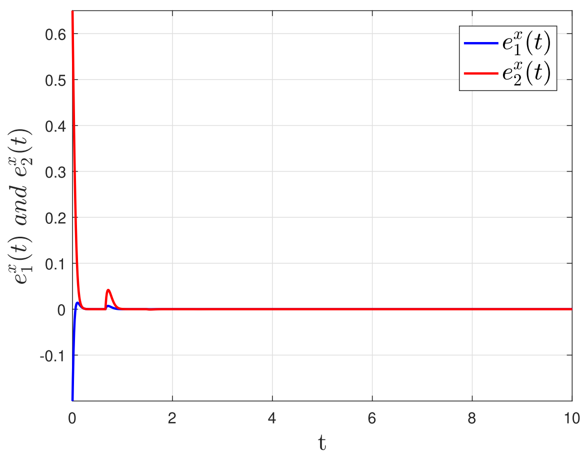

(b)

FIGURE 1. (a) The synchronization errors $e^x(t)$ without control. (b) The synchronization errors $e^x(t)$ under the controller (7).

Now combining (16) and (17), we get

$$
\begin{aligned}
\mathcal{L}V(t)=&\mathcal{L}V_1(t)+\mathcal{L}V_2(t)\\
\le&\sum_{i=1}^{n}\Big\{-(\lambda_{2i}+\min\{\delta_i\})(e_i^x(t))^2-\lambda_{3i}|e_i^x(t)|^{\varkappa+1}\\
&-\lambda_{4i}(\int_{t-\tau(t)}^{t}n_i(e_i^x(s))^2ds)^{\frac{\varkappa+1}{2}}
\end{aligned}
$$

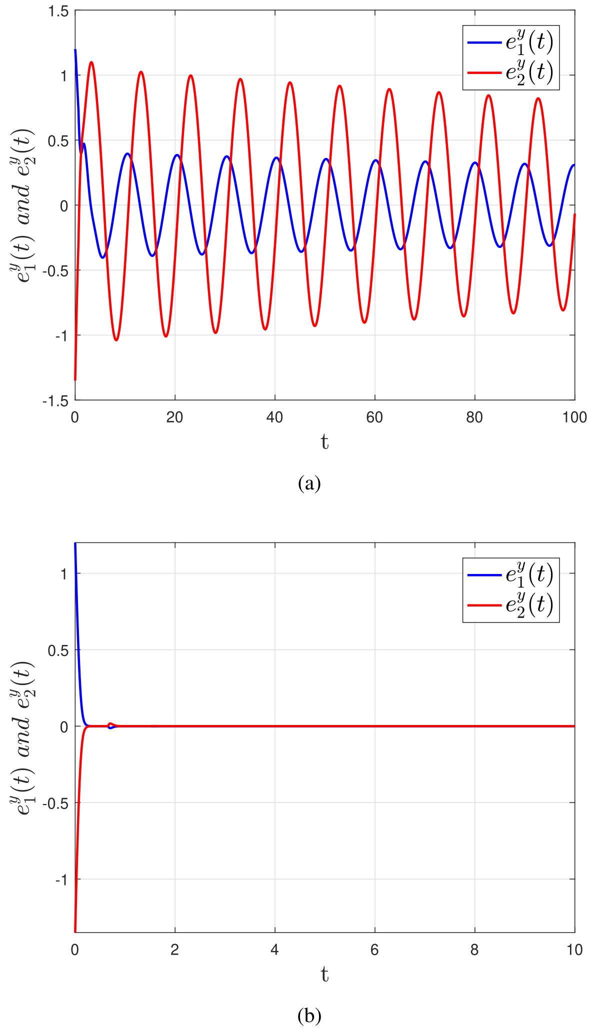

FIGURE 2. (a) The synchronization errors $e^y(t)$ without control. (b) The synchronization errors $e^y(t)$ under the controller (7).

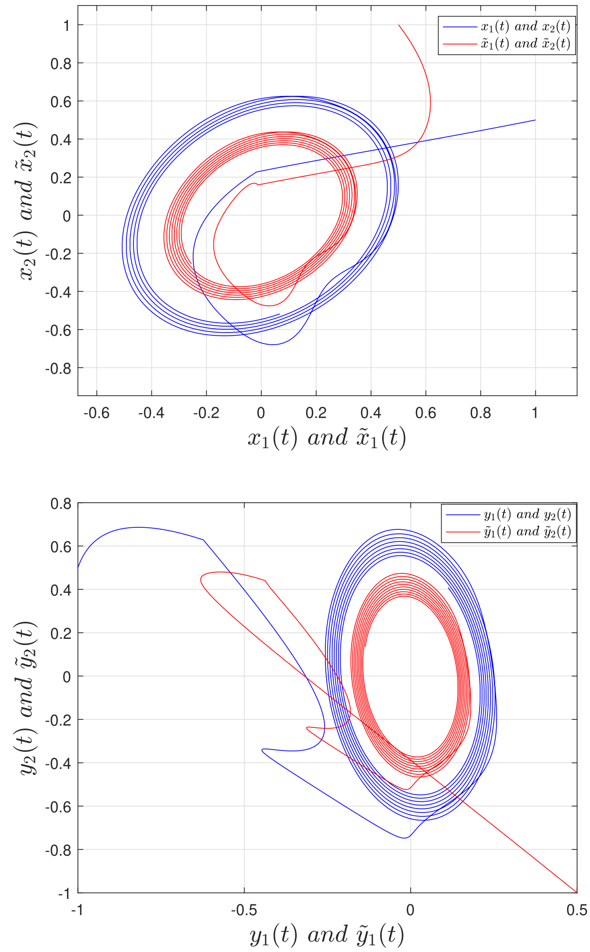

FIGURE 3. The chaotic attractors of the drive system (20) and response system (21).

$$
\begin{aligned}
&+\{(1+|\xi_i-1|)\left|\grave{\delta}_i-\acute{\delta}_i\right|T_i+\sum_{j=1}^{m}\Big[(\max\{a_{ji}\}\\
&+\max\{b_{ji}\})(1+\xi_i)p_j\Big]-\lambda_{1i}\}|e_i^x|\Big\}\\
&+\frac{1}{2}(e^y(t))^T(G_1+M)e^y(t)+\frac{1}{2}(e^y(t\\
&-\tau(t)))^T(G_2-(1-\tau)M)e^y(t-\tau(t))\\
&+\sum_{j=1}^{n}\{-(l_{2j}+\min\{\rho_j\})(e_j^y(t))^2-l_{3j}|e_j^y(t)|^{\varkappa+1}\\
&-l_{4j}(\int_{t-\tau(t)}^{t}m_j(e_j^y(s))^2ds)^{\frac{\varkappa+1}{2}}\\
&+\{(1+|\eta_j-1|)\left|\grave{\rho}_j-\acute{\rho}_j\right|\hat{T}_j+\sum_{i=1}^{n}\Big[(\max\{c_{ij}\}\\
&+\max\{d_{ij}\})(1+\eta_j)q_i\Big]\\
&-l_{1j}\}|e_j^y|\}+\frac{1}{2}(e^x(t))^T(H_1+N)e^x(t)+\frac{1}{2}(e^x(t\\
&-\tau(t)))^T(H_2-(1-\tau)N)e^x(t-\tau(t))
\end{aligned}
$$

$$
\begin{aligned}
\leq &\sum_{i=1}^{n}\{-(\lambda_{2i}+\min\{\delta_i\}-\frac{1}{2}h_{1i}-\frac{n_i}{2})(e_i^x(t))^2\\
&-\lambda_{3i}|e_i^x(t)|^{\varkappa+1}-\lambda_{4i}(\int_{t-\tau(t)}^{t}m_i(e_i^x(s))^2ds)^{\frac{\varkappa+1}{2}}\\
&+\{(1+|\xi_i-1|)\left|\grave{\delta}_i-\acute{\delta}_i\right|T_i+\sum_{j=1}^{m}\Big[(\max\{a_{ji}\}\\
&+\max\{b_{ji}\})(1+\xi_i)p_j\Big]-\lambda_{1i}\}|e_i^x|\}\\
&+\frac{1}{2}(e^y(t-\tau(t)))^T(G_2-(1-\tau)M)e^y(t-\tau(t))\\
&+\sum_{j=1}^{n}\{-(l_{2j}+\min\{\rho_j\}-\frac{1}{2}g_{1j}-\frac{m_j}{2})(e_j^y(t))^2\\
&-l_{3j}|e_j^y(t)|^{\varkappa+1}-l_{4j}(\int_{t-\tau(t)}^{t}n_j(e_j^y(s))^2ds)^{\frac{\varkappa+1}{2}}\\
&+\{(1+|\eta_j-1|)\left|\grave{\rho}_j-\acute{\rho}_j\right|\hat{T}_j+\sum_{i=1}^{n}\Big[(\max\{c_{ij}\}\\
&+\max\{d_{ij}\})(1+\eta_j)q_i\Big]-l_{1j}\}|e_j^y|\}\\
&+\frac{1}{2}(e^x(t-\tau(t)))^T(H_2-(1-\tau)N)e^x(t-\tau(t)).
\end{aligned}
$$

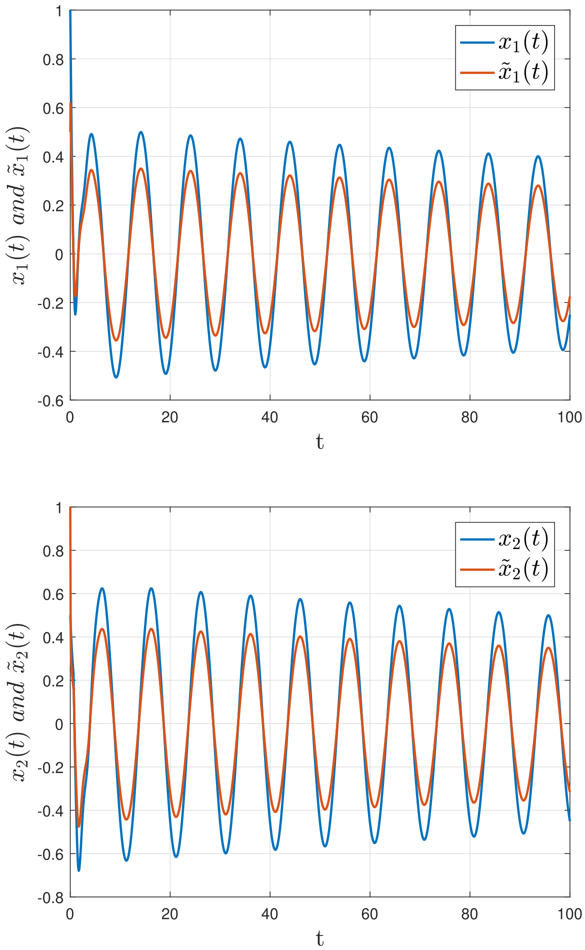

FIGURE 4. The dynamic behavior of state x in drive-response system.

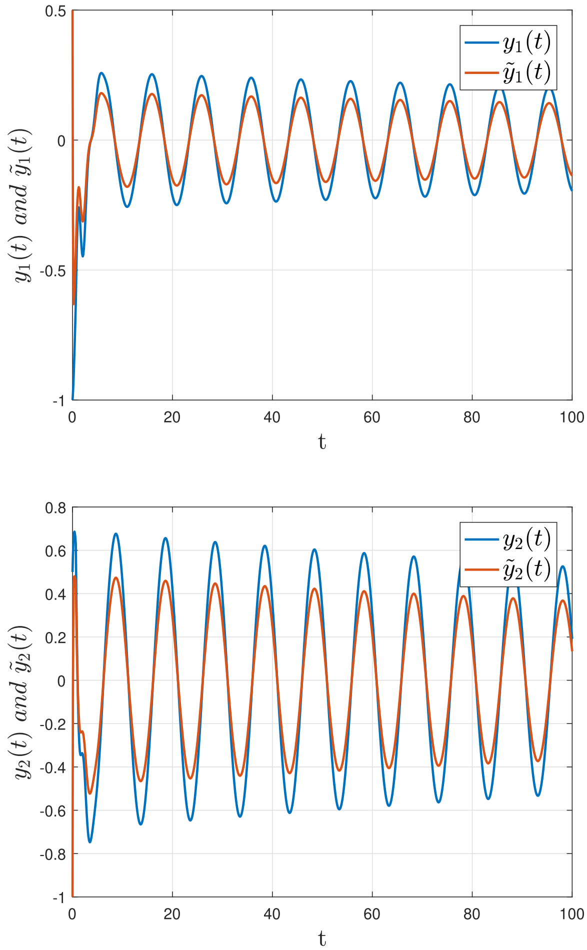

FIGURE 5. The dynamic behavior of state y in drive-response system.

Since λ_{1i}, λ_{2i}, l_{1j}, l_{2j} satisfy the conditions in (15), letting $G_2 = (1-\tau)M$ and $H_2 = (1-\tau)N$, we obtain

$$\begin{cases} \lambda_{2i} > -\min\{\delta_i\} + \frac{h_{1i}}{2} + \frac{h_{2i}}{2} \\ \quad \Leftrightarrow \lambda_{2i} > -\min\{\delta_i\} + \frac{h_{1i}}{2} + \frac{n_i}{2}, \\ l_{2j} > -\min\{\rho_j\} + \frac{g_{1j}}{2} + \frac{g_{2j}}{2} \\ \quad \Leftrightarrow l_{2j} > -\min\{\rho_j\} + \frac{g_{1j}}{2} + \frac{m_j}{2}. \end{cases}$$

Applying Lemma 6, we can get

$$\begin{aligned} \mathcal{L}V \le \sum_{i=1}^{n} \Big\{ & -\lambda_{3i}|e_i^x(t)|^{\varkappa+1} \\ & -\lambda_{4i}\Big(\int_{t-\tau(t)}^{t} m_i(e_i^x(s))^2 ds\Big)^{\frac{\varkappa+1}{2}} \Big\} \\ & + \sum_{i=1}^{n} \Big\{ -l_{3j}|e_j^y(t)|^{\varkappa+1} \\ & -l_{4j}\Big(\int_{t-\tau(t)}^{t} n_j(e_j^y(s))^2 ds\Big)^{\frac{\varkappa+1}{2}} \Big\} \end{aligned}$$

$$\begin{aligned} & \le -2^{\frac{\varkappa+1}{2}}\Big(\sum_{i=1}^{n}\frac{\lambda_{3i}}{2}(e_i^x(t))^2 + \sum_{j=1}^{m}\frac{\text{ł}_{3j}}{2}(e_j^y(t))^2\Big)^{\frac{\varkappa+1}{2}} \\ & \quad - 2^{\frac{\varkappa+1}{2}}\Big(\frac{1}{2}\int_{t-\tau(t)}^{t}(e^x(s))^T M e^x(s)ds\Big)^{\frac{\varkappa+1}{2}} \\ & \quad - 2^{\frac{\varkappa+1}{2}}\Big(\frac{1}{2}\int_{t-\tau(t)}^{t}(e^y(s))^T N e^y(s)ds\Big)^{\frac{\varkappa+1}{2}} \\ & \le -2^{\frac{\varkappa+1}{2}}(min_{i,j}\{\lambda_{3i}, \lambda_{4i}, \text{ł}_{3j}, l_{4j}\})(V(t))^{\frac{\varkappa+1}{2}}. \end{aligned} \tag{18}$$

According to Lemma 5, system (1) and (3) achieve function projective synchronization. Therefore,

$$E[V] \le -2^{\frac{\varkappa+1}{2}}(min_{i,j}\{\lambda_{3i}, \lambda_{4i}, \text{ł}_{3j}, l_{4j}\})(E[V(t)])^{\frac{\varkappa+1}{2}}. \tag{19}$$

By Lemma 7, $E[V(t)]$ stochastically converges to zero in a finite time, and the finite time is estimated by $t_1 = \frac{V^{1-\frac{\varkappa+1}{2}}(0)}{2^{\frac{\varkappa+1}{2}}(min_{i,j}\{\lambda_{3i},\lambda_{4i},\text{ł}_{3j},l_{4j}\})(1-\frac{\varkappa+1}{2})}$. Hence, system (1) and (3) can projectively synchronize under stochastic perturbations in finte-time. This completes the proof. □

Remark 1: In Theorem 1, we only consider the finite-time projective synchronization with time delays of system.

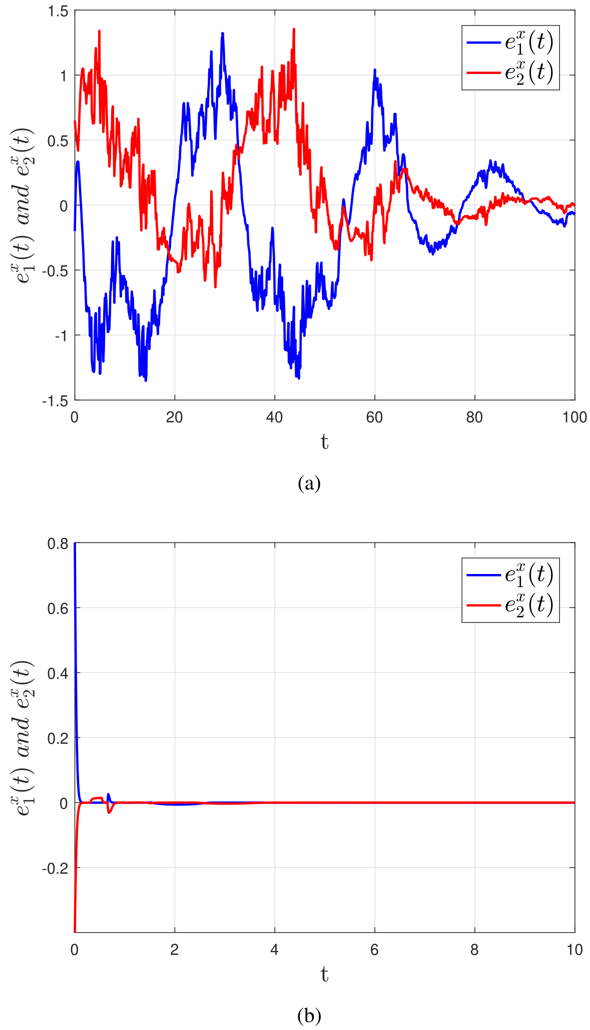

FIGURE 6. (a) The synchronization errors $e^x(t)$ without control, (b) The synchronization errors $e^x(t)$ under the controller (13)**.**

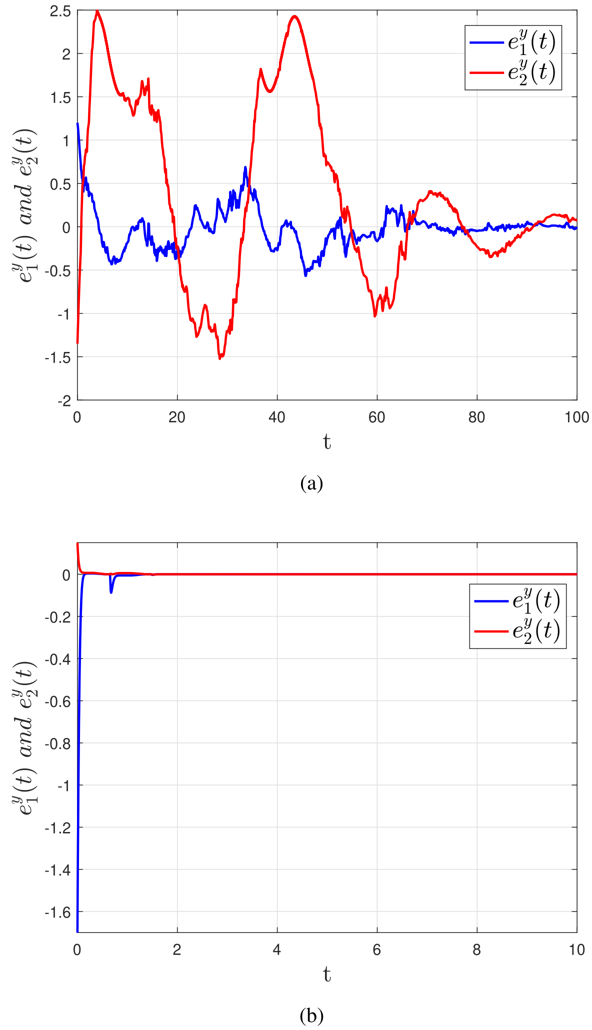

FIGURE 7. (a) The synchronization errors $e^y(t)$ without control. (b) The synchronization errors $e^y(t)$ under the controller (13)**.**

However, we take into account consider the stochastic perturbations system in Theorem 2.

Remark 2: Stochastic perturbations are inevitable and may lead to instability of system in real nervous systems. Therefore, it is of great essence to consider stochastic perturbations in MBAMNNs as our analysis in Theorem 2.

Remark 3: In the controllers (7) and (14), the discontinuous terms sign(e(t)) may be undesirable in practical applications.In this case, the continuous terms $\frac{e(t)}{e(t)+k}$ can be chosen as approximations of sign(e(t)), in which k > 0 is sufficiently small.

IV. NUMERICAL SIMULATIONS

In this section, three numerical simulations are given to show the effectiveness of the obtained results and the potential applications in image encryption.

Example 1: Here we consider the following memristor-based BAM neural networks with $n = 2$ and $m = 2$ as drive system

$$\begin{cases} dx_i(t) = [-\delta_i(x_i(t))x_i(t) + \sum_{j=1}^{2} a_{ji}(x_i(t))f_j(y_j(t)) \\ \qquad + \sum_{j=1}^{2} b_{ji}(x_i(t))f_j(y_j(t-\tau(t)))]dt, \\ dy_j(t) = [-\rho_i(y_j(t))y_j(t) + \sum_{i=1}^{2} c_{ij}(y_j(t))g_j(x_j(t)) \\ \qquad + \sum_{i=1}^{2} d_{ij}(y_j(t))g_j(x_j(t-\tau(t)))]dt, \end{cases} \tag{20}$$

with the following parameters

$$\delta_1(\gamma) = \begin{cases} 1.5, & |\gamma| < 1, \\ 2, & |\gamma| > 1, \end{cases} \quad \delta_2(\gamma) = \begin{cases} 0.9, & |\gamma| < 1, \\ 0.8, & |\gamma| > 1, \end{cases}$$

$$a_{11}(\gamma) = \begin{cases} -0.3, & |\gamma| < 1, \\ 1.5, & |\gamma| > 1, \end{cases} \quad a_{12}(\gamma) = \begin{cases} 0.2, & |\gamma| < 1, \\ 1, & |\gamma| > 1, \end{cases}$$

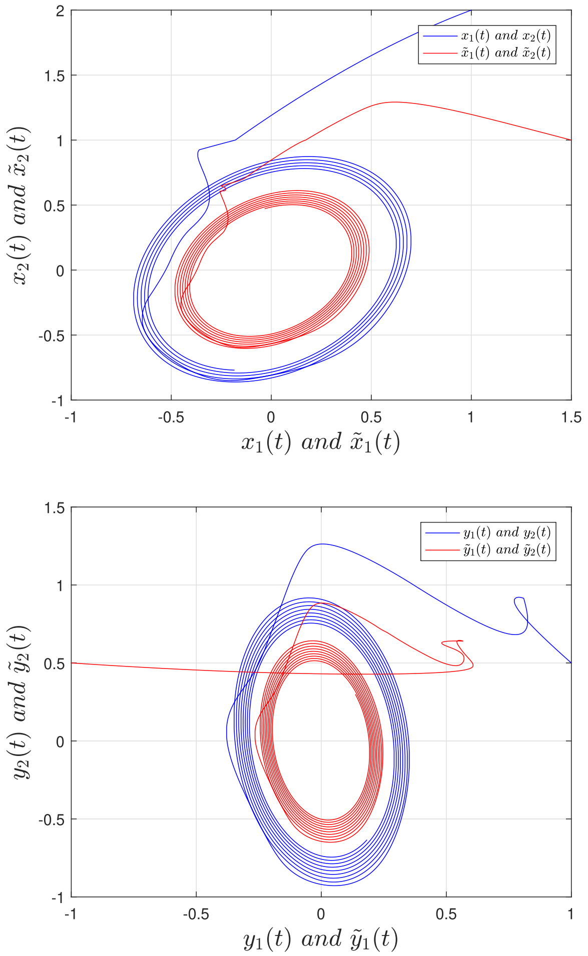

FIGURE 8. The chaotic attractors of the drive system (20) and response system (22).

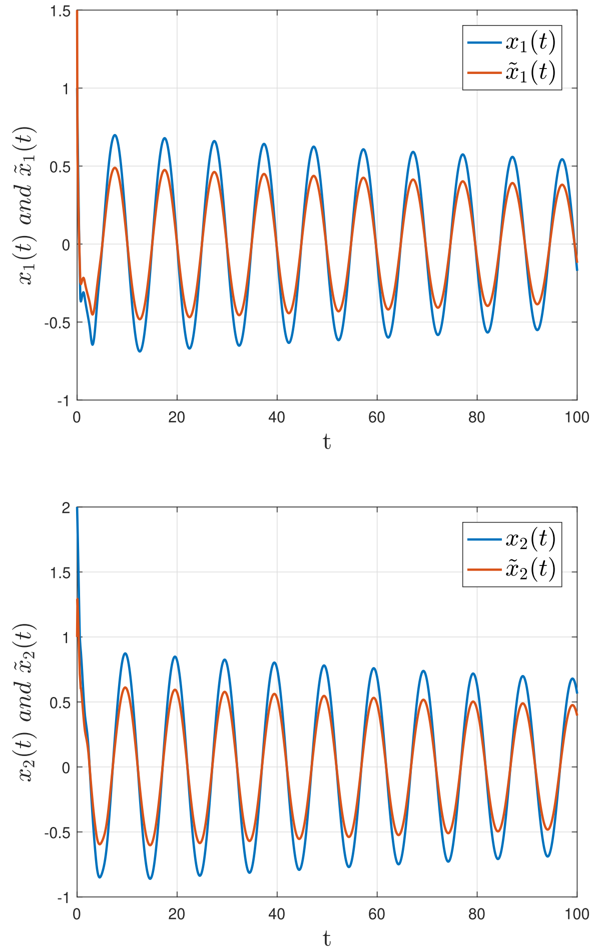

FIGURE 9. The dynamic behavior of state x in drive-response system.

$$a_{21}(\gamma)=\begin{cases}-1.8, & |\gamma|<1,\\ 0.8, & |\gamma|>1,\end{cases}\quad a_{22}(\gamma)=\begin{cases}0.1, & |\gamma|<1,\\ -1.9, & |\gamma|>1,\end{cases}$$

$$b_{11}(\gamma)=\begin{cases}0.9, & |\gamma|<1,\\ 1.7, & |\gamma|>1,\end{cases}\quad b_{12}(\gamma)=\begin{cases}0.7, & |\gamma|<1,\\ 1.5, & |\gamma|>1,\end{cases}$$

$$b_{21}(\gamma)=\begin{cases}0.5, & |\gamma|<1,\\ -0.3, & |\gamma|>1,\end{cases}\quad b_{22}(\gamma)=\begin{cases}-0.95, & |\gamma|<1,\\ 1, & |\gamma|>1,\end{cases}$$

$$\rho_{1}(\gamma)=\begin{cases}0.9, & |\gamma|<2,\\ 1, & |\gamma|>2,\end{cases}\quad \rho_{2}(\gamma)=\begin{cases}1, & |\gamma|<2,\\ 0.8, & |\gamma|>2,\end{cases}$$

$$c_{11}(\gamma)=\begin{cases}-1, & |\gamma|<2,\\ 0.7, & |\gamma|>2,\end{cases}\quad c_{12}(\gamma)=\begin{cases}1, & |\gamma|<2,\\ 1, & |\gamma|>2,\end{cases}$$

$$c_{21}(\gamma)=\begin{cases}0.7, & |\gamma|<2,\\ -1, & |\gamma|>2,\end{cases}\quad c_{22}(\gamma)=\begin{cases}1.2, & |\gamma|<2,\\ 0.5, & |\gamma|>2,\end{cases}$$

$$d_{11}(\gamma)=\begin{cases}1, & |\gamma|<2,\\ -1, & |\gamma|>2,\end{cases}\quad d_{12}(\gamma)=\begin{cases}-2.4, & |\gamma|<2,\\ 0.5, & |\gamma|>2,\end{cases}$$

$$d_{21}(\gamma)=\begin{cases}-1, & |\gamma|<2,\\ 1, & |\gamma|>2,\end{cases}\quad d_{22}(\gamma)=\begin{cases}1, & |\gamma|<2,\\ -1, & |\gamma|>2.\end{cases}$$

The activation functions are $f_1(\gamma) = f_2(\gamma) = g_1(\gamma) = g_2(\gamma) = \frac{|\gamma+1|-|\gamma-1|}{2}$; $p_j = q_i = 1$; $\alpha_1(t) = \alpha_2(t) = \beta_1(t) = \beta_2(t) = 0.7$; $\tau(t) = \frac{e^t}{e^t+1}$. The initial values of (20) are $\psi(s) = (1, 0.5)^T$ and $\phi(s) = (-1, 0.5)^T$.

For drive system (20), we construct the corresponding response system as

$$\begin{cases} d\tilde{x}_i(t) = [-\delta_i(\tilde{x}_i(t))\tilde{x}_i(t) + \sum_{j=1}^{2} a_{ji}(\tilde{x}_i(t))f_j(\tilde{y}_j(t)) \\ \qquad + \sum_{j=1}^{2} b_{ji}(\tilde{x}_i(t))f_j(\tilde{y}_j(t-\tau(t))) + u_i(t)]dt, \\ d\tilde{y}_j(t) = [-\rho_i(\tilde{y}_j(t))\tilde{y}_j(t) + \sum_{i=1}^{2} c_{ij}(\tilde{y}_j(t))g_j(\tilde{x}_j(t)) \\ \qquad + \sum_{i=1}^{2} d_{ij}(\tilde{y}_j(t))g_j(\tilde{x}_j(t-\tau(t))) + v_j(t)]dt. \end{cases} \tag{21}$$

The initial values of (21) are $\tilde{\psi}(s) = (0.5, 1)^T$ and $\tilde{\phi}(s) = (0.5, -1)^T$.

According to Theorem 1, it can be calculated that $\lambda_{11} > 7.8$, $\lambda_{12} > 7.15$, $\lambda_{21} > -1.5$, $\lambda_{22} > -0.8$, $l_{11} > 5.46$, $l_{12} > 7.54$, $l_{21} > -0.9$, $l_{22} > -0.8$. Therefore, we choose

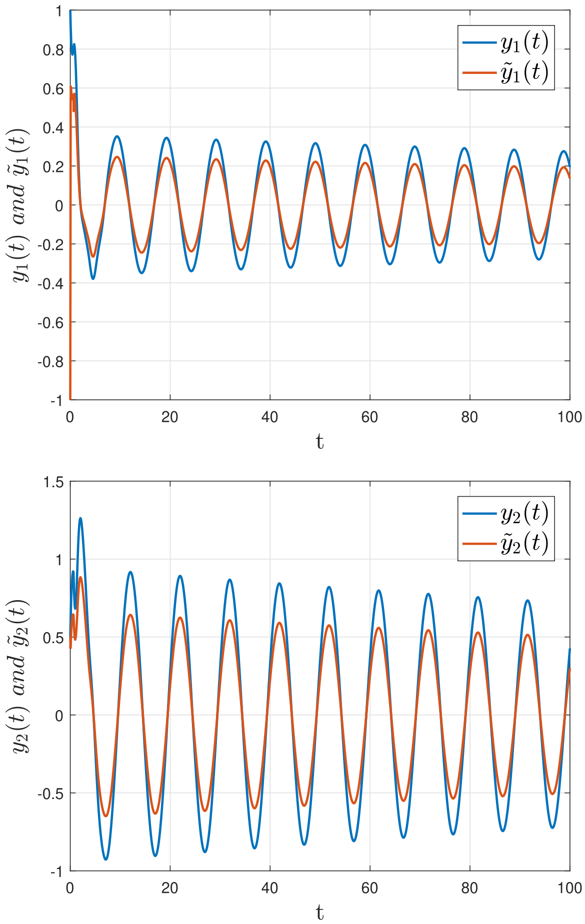

FIGURE 10. The dynamic behavior of state y in drive-response system.

FIGURE 11. (a) The color plain image. (b-c-d) The R, G, B components of plain image.

$\lambda_{11} = 10$, $\lambda_{12} = 8$, $\lambda_{21} = 1$, $\lambda_{22} = 1$, $\lambda_{31} = 0.5$, $\lambda_{32} = 0.5$, $l_{11} = 6$, $l_{12} = 8$, $l_{21} = 0.5$, $l_{22} = 1$, $l_{31} = 0.5$, $l_{32} = 0.5$, $\varkappa = 0.6$, then the settling time $t_1 = 6.50$.

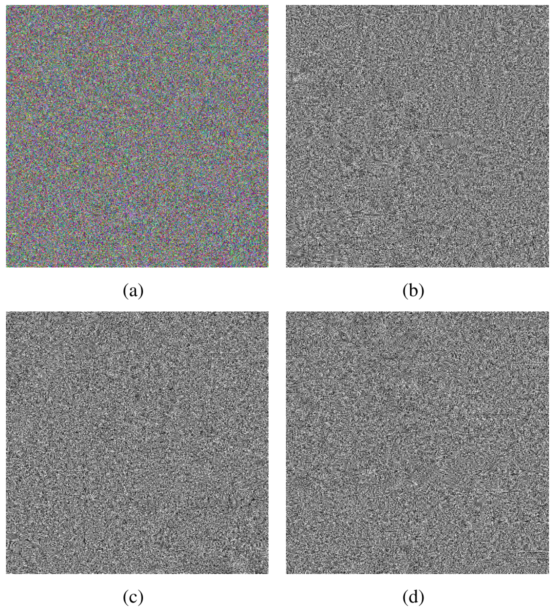

FIGURE 12. (a) The encrypted image. (b-c-d) the R, G, B components of encrypted image.

The dynamic behavior of state x in drive-response system is shown in Fig. 4 and the dynamic behavior of state y in drive-response system is presented in Fig. 5.

Fig. 1(a) and Fig. 2(a) show the state trajectories of synchronization errors $e^x(t)$ and $e^y(t)$ without controller, respectively. Fig. 1(b) and Fig. 2(b) show the synchronization errors $e^x(t)$ and $e^y(t)$ under the feedback controllers (7), respectively. From these two figures, we can see that synchronization errors $e^x(t)$ and $e^y(t)$ are converge to zero within finite-time 6.50, which shows the finite-time projective synchronization achieved between system (20) and (21). The effectiveness of Theorem 1 is verified.

The chaotic attractors of the drive system and response system are given in Fig. 3. From Fig. 3, it can be seen that (20) and (21) are great chaotic systems and can be effectively employed in chaotic image algorithms.

Example 2: For drive system (20), we consider the stochastic perturbations in response system as follows

$$\begin{cases} d\tilde{x}_i(t) = [-\delta_i(\tilde{x}_i(t))\tilde{x}_i(t) + \sum_{j=1}^{2} a_{ji}(\tilde{x}_i(t))f_j(\tilde{y}_j(t)) \\ \qquad + \sum_{j=1}^{2} b_{ji}(\tilde{x}_i(t))f_j(\tilde{y}_j(t-\tau(t))) + u_i(t)]dt \\ \qquad + \sum_{j=1}^{2} \sigma_{ji}(t, e_j^y(t), e_j^y(t-\tau(t))d\omega_j(t), \\ d\tilde{y}_j(t) = [-\rho_i(\tilde{y}_j(t))\tilde{y}_j(t) + \sum_{i=1}^{2} c_{ij}(\tilde{y}_j(t))g_j(\tilde{x}_j(t)) \\ \qquad + \sum_{i=1}^{2} d_{ij}(\tilde{y}_j(t))g_j(\tilde{x}_j(t-\tau(t))) + v_j(t)]dt \\ \qquad + \sum_{i=1}^{2} \tilde{\sigma}_{ij}(t, e_i^x(t), e_i^x(t-\tau(t))d\tilde{\omega}_i(t). \end{cases} \tag{22}$$

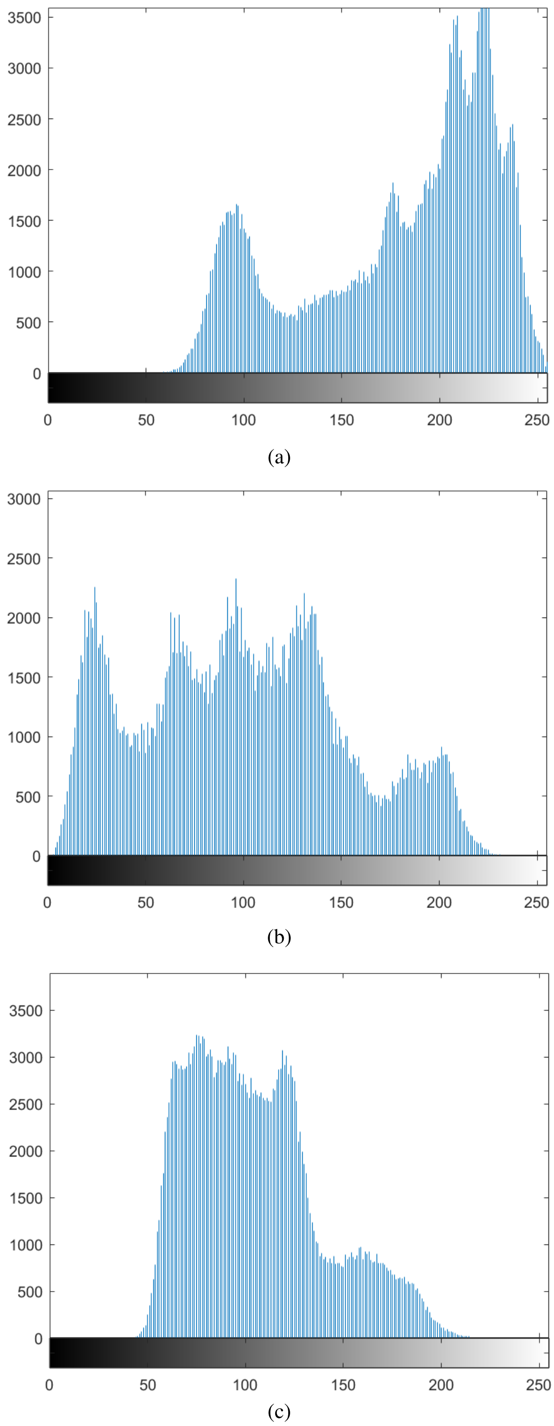

FIGURE 13. Histogram of the plain image. (a) Histogram of R components of the plain image. (b) Histogram of G components of the plain image. (c) Histogram of B components of the plain image.

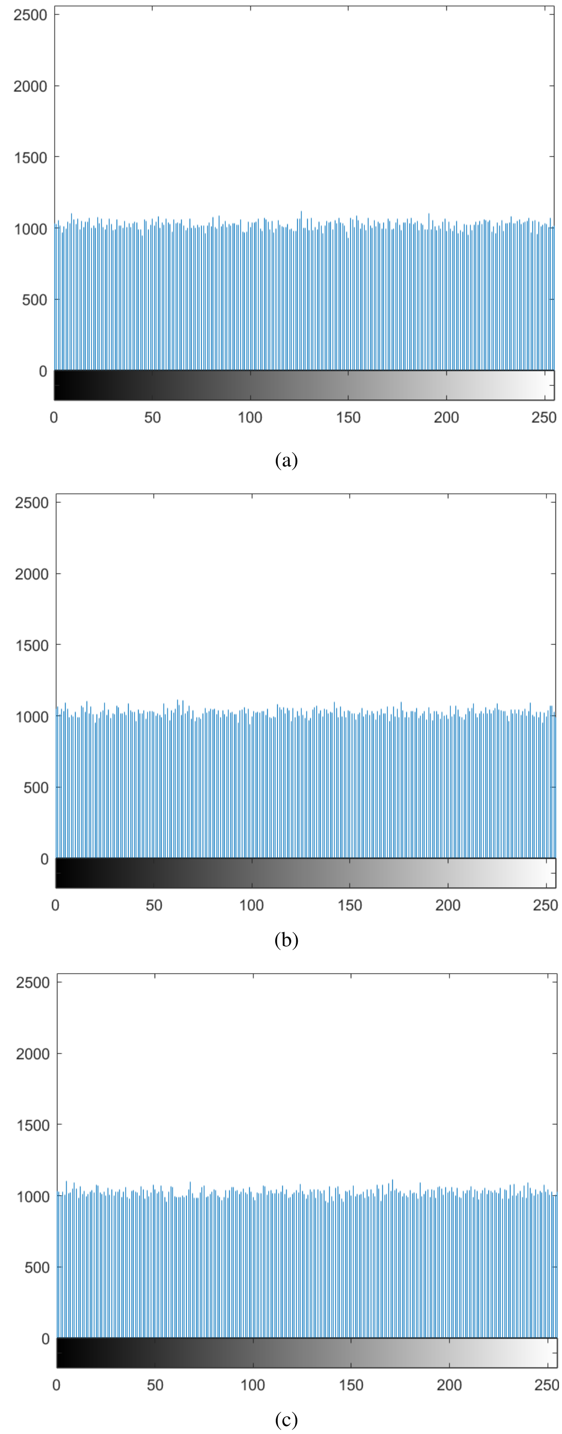

FIGURE 14. Histogram of the encrypted image. (a) Histogram of R components of the encrypted image. (b) Histogram of G components of the encrypted image.
(c) Histogram of B components of the encrypted image.

The activation functions are $f_1(\gamma) = f_2(\gamma) = g_1(\gamma) = g_2(\gamma) = \frac{|\gamma+1|-|\gamma-1|}{2}$; $p_j = q_i = 1$; $\alpha_1(t) = \alpha_2(t) = \beta_1(t) = \beta_2(t) = 0.7$; $\tau(t) = \frac{e^t}{e^t+1}$, $\dot{\tau}(t) \leq 0.25 < \tau = 0.5$. Moreover, we assume the initial values of drive system (20) are $\psi(s) = (1, 2)^T$, $\phi(s) = (1, 0.5)^T$ and the initial values $\tilde{\psi}(s) = (1.5, 1)^T$, $\tilde{\phi}(s) = (-1, 0.5)^T$.

Let $\sigma(t, e(t), e(t-\tau(t))) = \tilde{\sigma}(t, e(t), e(t-\tau(t))) = \begin{pmatrix} 0.4e(t-\tau(t)) & 0.4e(t-\tau(t)) \\ 0.7e(t-\tau(t)) & 0.7e(t-\tau(t)) \end{pmatrix}$ and we get $G_1 = H_1 = diag(0, 0)$, $G_2 = H_2 = diag(0.16, 0.49)$.

According to Theorem 2, it can be calculated that $\lambda_{11} > 7.8$, $\lambda_{12} > 7.15$, $\lambda_{21} > -1.34$, $\lambda_{22} > -0.31$, $l_{11} > 5.46$, $l_{12} > 7.54$, $l_{21} > -0.74$, $l_{22} > -0.31$. Therefore, we choose

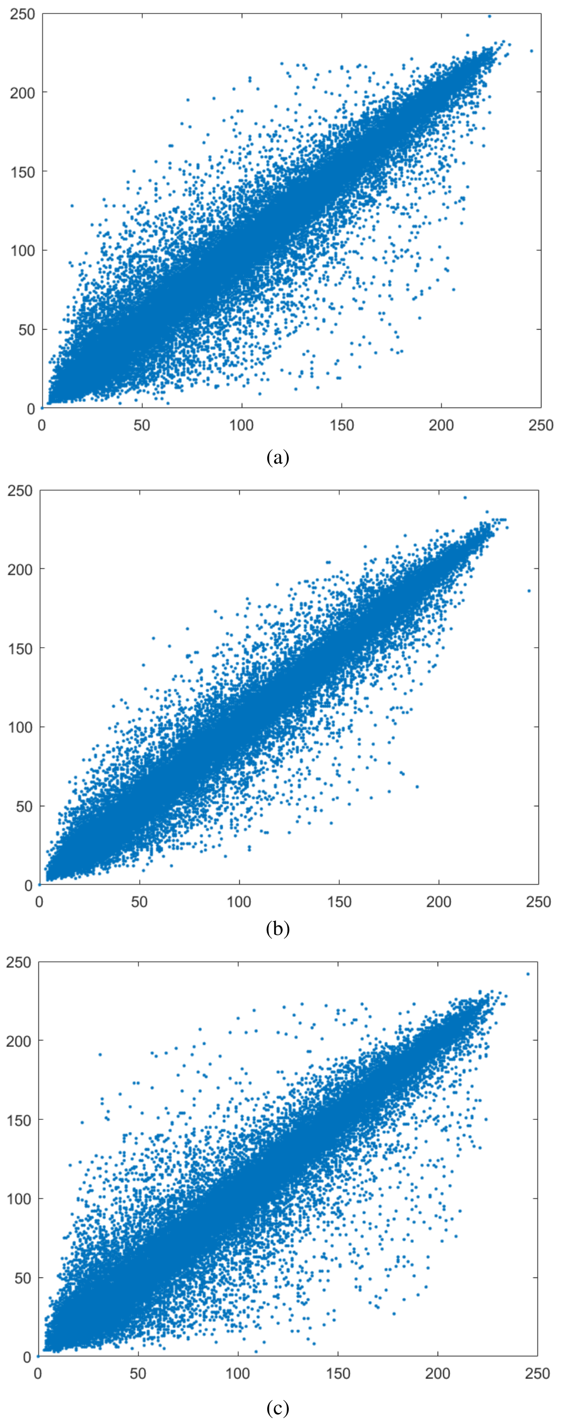

FIGURE 15. Correlation of neighborhood pixels at different directions of the plain image. (a) Horizontal directions. (b) Vertical directions. (c) Diagonal directions.

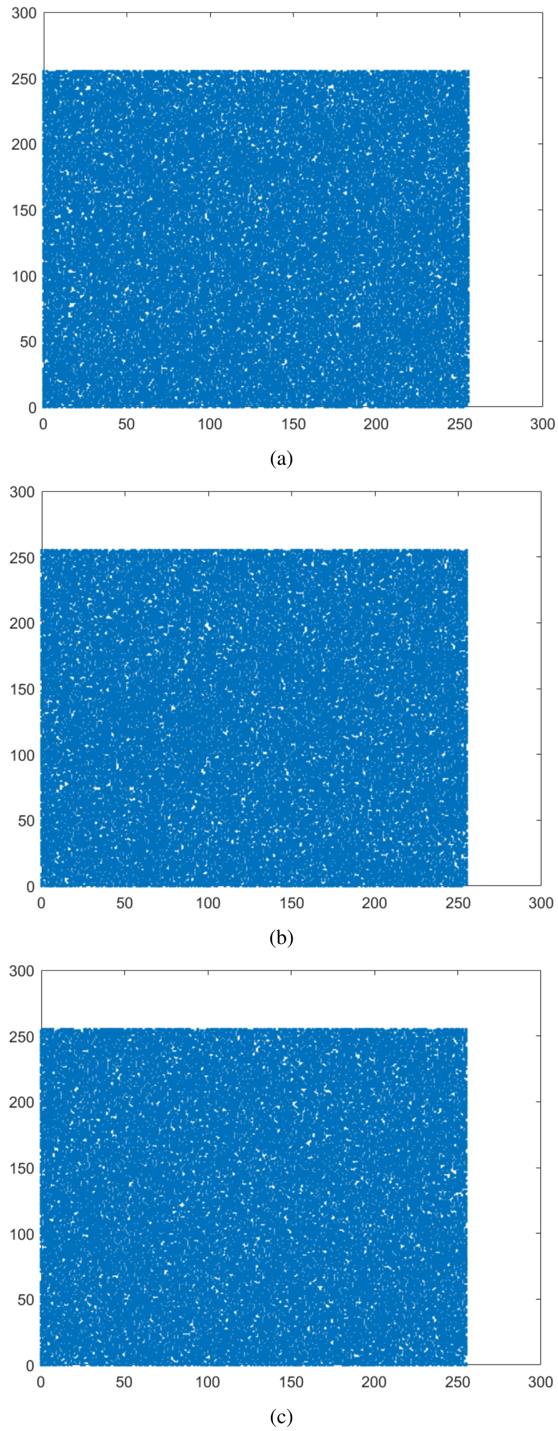

FIGURE 16. Correlation of neighborhood pixels at different directions of the encrypted image. (a) Horizontal directions. (b) Vertical directions. (c) Diagonal directions.

$\lambda_{11} = 8$, $\lambda_{12} = 7.5$, $\lambda_{21} = 1$, $\lambda_{22} = 1$, $\lambda_{31} = 0.5$, $\lambda_{32} = 0.5$, $\lambda_{41} = 0.5$, $\lambda_{42} = 0.5$, $l_{11} = 6$, $l_{12} = 8$, $l_{21} = 0.5$, $l_{22} = 1$, $l_{31} = 0.5$, $l_{32} = 0.5$, $l_{41} = 0.5$, $l_{42} = 0.5$, $\varkappa = 0.6$, then the settling time $t_1 = 6.50$.

Fig. 6(a) and Fig. 7(a) show the state trajectories of synchronization errors $e^x(t)$ and $e^y(t)$ without controller, respectively. Synchronization errors $e^x(t)$ and $e^y(t)$ under the feedback controllers (7) are presented in Fig. 6(b) and Fig. 7(b), respectively. These two figures indicate that the projective synchronization achieves within finite-time $t_1 = 6.50$, which illustrates the effectiveness of the obtained results in Theorem 2.

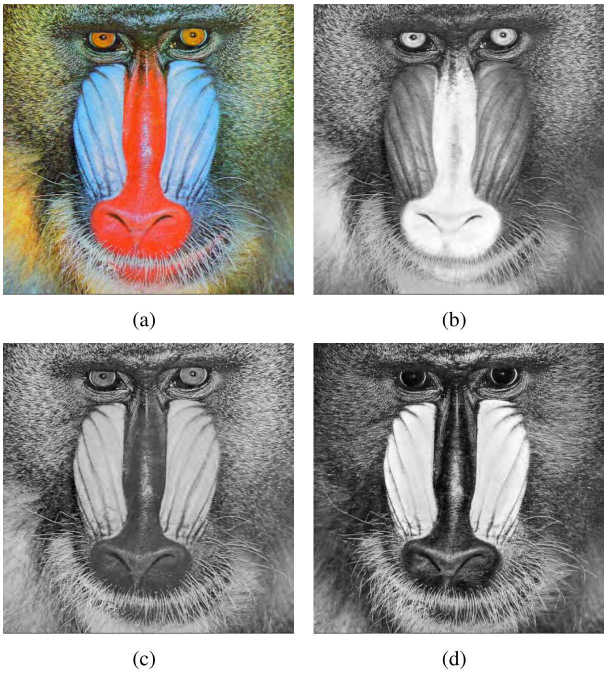

FIGURE 17. (a) The color plain image. (b-c-d) The R, G, B components of plain image.

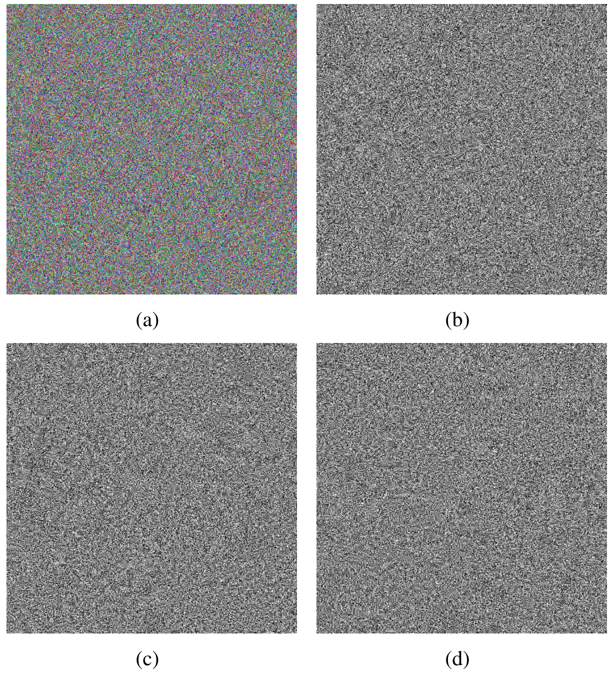

FIGURE 18. (a) The encrypted image. (b-c-d) the R, G, B components of encrypted image.

Dynamic behavior of state x in drive-response system is presented in Fig. 9 and the dynamic behavior of state y in drive-response system is shown in Fig. 10.

The chaotic attractors of the drive and response systems are given in Fig. 8. From Fig. 8, it can be seen that (20) and (22) are systems with strong chaotic properties and can be employed in chaotic image algorithms effectively.

Example 3: Memristor-based BAM neural networks in Example 1 has greate chaotic attractor, and it can be applied to image encryption. Simulation results obtained from Example 1 can be used in image encryption. We assume that the size of the color plain image P is $m \times n \times 3$. The details about the encryption algorithm is introduced as follows

Algorithm 1 Encryption

$i := 1; j := 1; k := 1;$
for i to m **do**
  for j to n **do**
    $z_1(i,j) := \left(10^8 \times (z_1(k) - [z_1(k)])\right) \bmod 256;$
    $z_2(i,j) := \left(10^8 \times (z_2(k) - [z_2(k)])\right) \bmod 256;$
    $z_3(i,j) := \left(10^8 \times (z_3(k) - [z_3(k)])\right) \bmod 256;$
    $R(i,j) := R(i,j)\ XOR\ z_1(i,j);$
    $G(i,j) := G(i,j)\ XOR\ z_2(i,j);$
    $B(i,j) := B(i,j)\ XOR\ z_3(i,j);$
  end for
end for

1) The drive system (20) in Example 1 generates four chaotic sequences denoted by X_1, X_2, Y_1, Y_2 , and their size is $m \times n$. Since the color plain image P is consisted of three channels: red, green and blue, we separate it into three pixel sequences: $R(i,j)$, $G(i,j)$ and $B(i,j)$, where $i = 1, 2, \ldots, m, j = 1, 2, \ldots n$.
2) Now we apply the permutation operation to color plain image. We arrange the chaotic sequence X_1 in ascending order to obtain the index sequence *idx* of the sorted X_1. The permutation operation is described as follows
$$\begin{aligned}\hat{R}(k) &:= R(idx((i-1) \times n + j)),\\ \hat{G}(k) &:= G(idx((i-1) \times n + j)),\\ \hat{B}(k) &:= B(idx((i-1) \times n + j)),\\ R(i,j) &:= \hat{R}(k), \quad G(k) := \hat{G}(k),\ B(k) := \hat{B}(k).\end{aligned}$$
where $k = 1, 2, \ldots, mn$, $i = 1, 2, \ldots, n$, $j = 1, 2, \ldots, m$; $\hat{R}$, $\hat{G}$, $\hat{B}$ are sequences with the size of $m \times n$.
3) We transform chaotic sequence X_2, Y_1, Y_2 into $m \times n$ matrices z_1, z_2, z_3 as follows
$$\begin{cases} z_1(i,j) := X_2(k),\\ z_2(i,j) := Y_1(k),\\ z_3(i,j) := Y_2(k). \end{cases}$$
4) Now we use z_1, z_2, z_3 to encrypt the permuted $R(i,j)$, $G(i,j)$, $B(i,j)$ according to Algorithm 1, respectively. After reorganizing $R(i,j)$, $G(i,j)$, $B(i,j)$, the encrypted image is obtained. It should be noted that $[z_i(k)]$ is equivalent to $floor(z_i(k))$.

Decryption process is the reverse of encryption process, so it is omitted here. It should be noted that the decryption process should use chaotic sequences generated by response system (21). Fig. 11 and Fig. 12 show the color plain image and encrypted image, respectively.

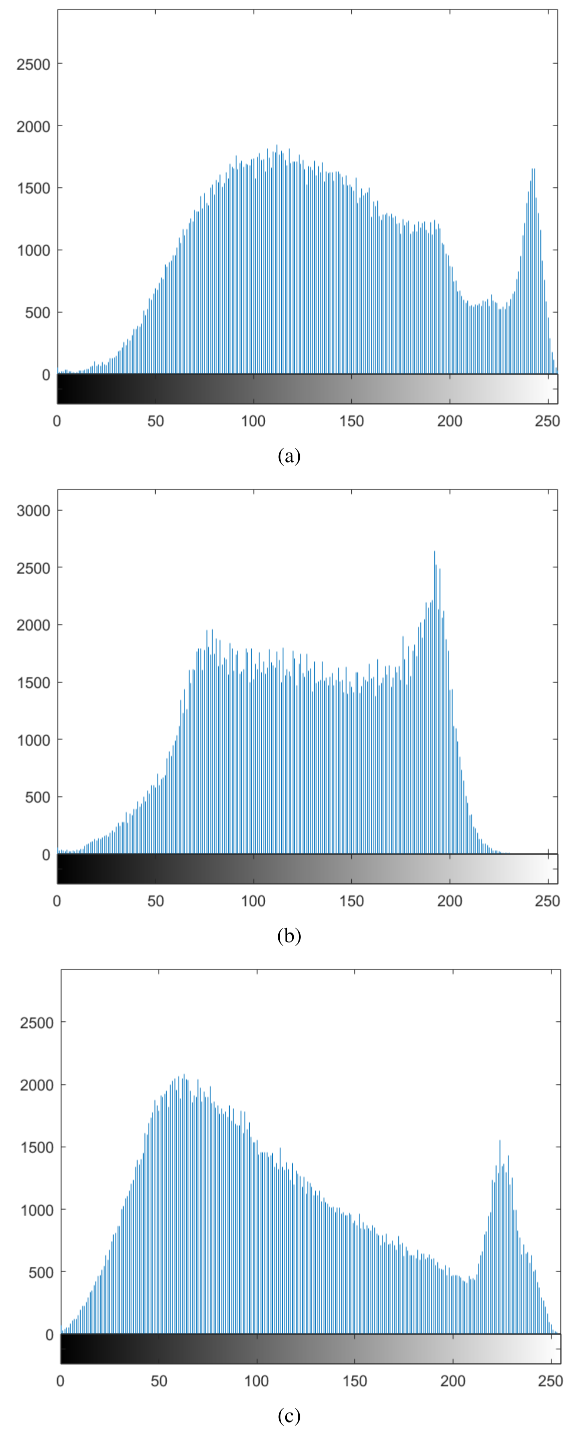

FIGURE 19. **Histogram of the plain image. (a) Histogram of R components of the plain image. (b) Histogram of G components of the plain image. (c) Histogram of B components of the plain image.**

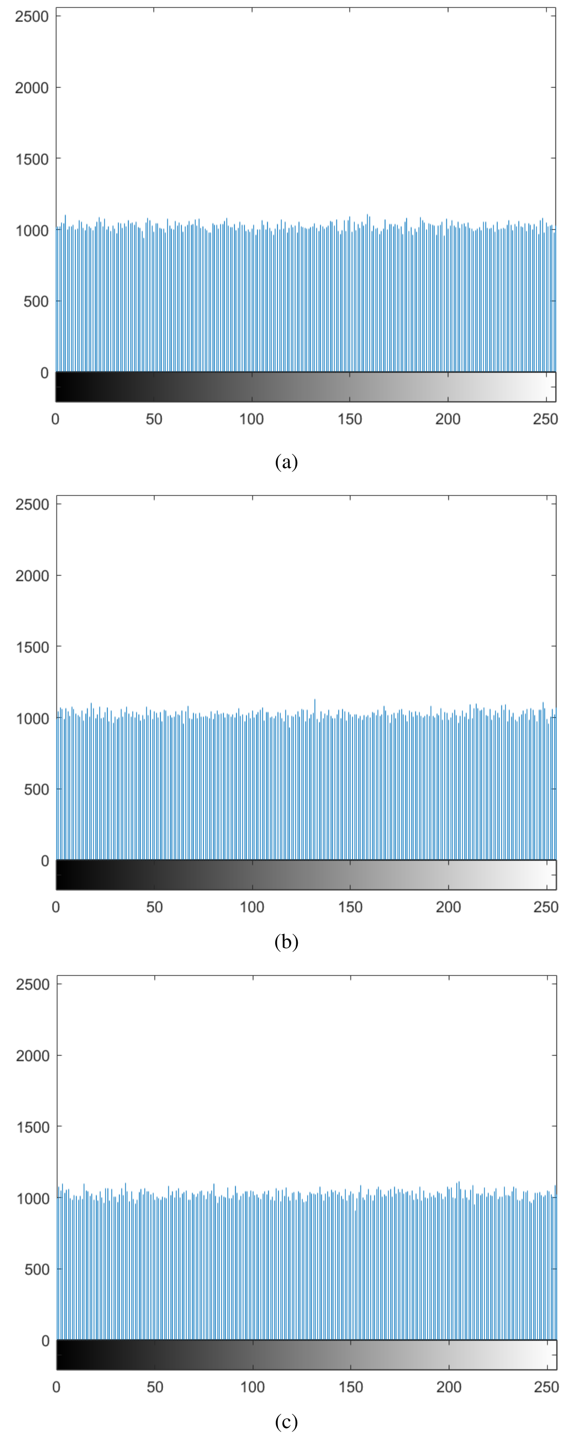

FIGURE 20. **Histogram of the encrypted image. (a) Histogram of R components of the encrypted image. (b) Histogram of G components of the encrypted image. (c) Histogram of B components of the encrypted image.**

From Fig. 14, we find that the histograms of the encrypted image are uniformly distributed and different from the histograms of the plain image shown in Fig. 13. The uniformly distribution means that the encrypted image does not provide any information about the plain image and the proposed encryption algorithm can resist statistical attack.

The correlations of neighborhood pixels at different directions (horizontal-vertical-diagonal) of the plain image and encrypted image are shown in Fig. 15 and 16. From Fig. 15, it can be seen that the plain image has strong correlations between neighborhood pixels, while correlations of the

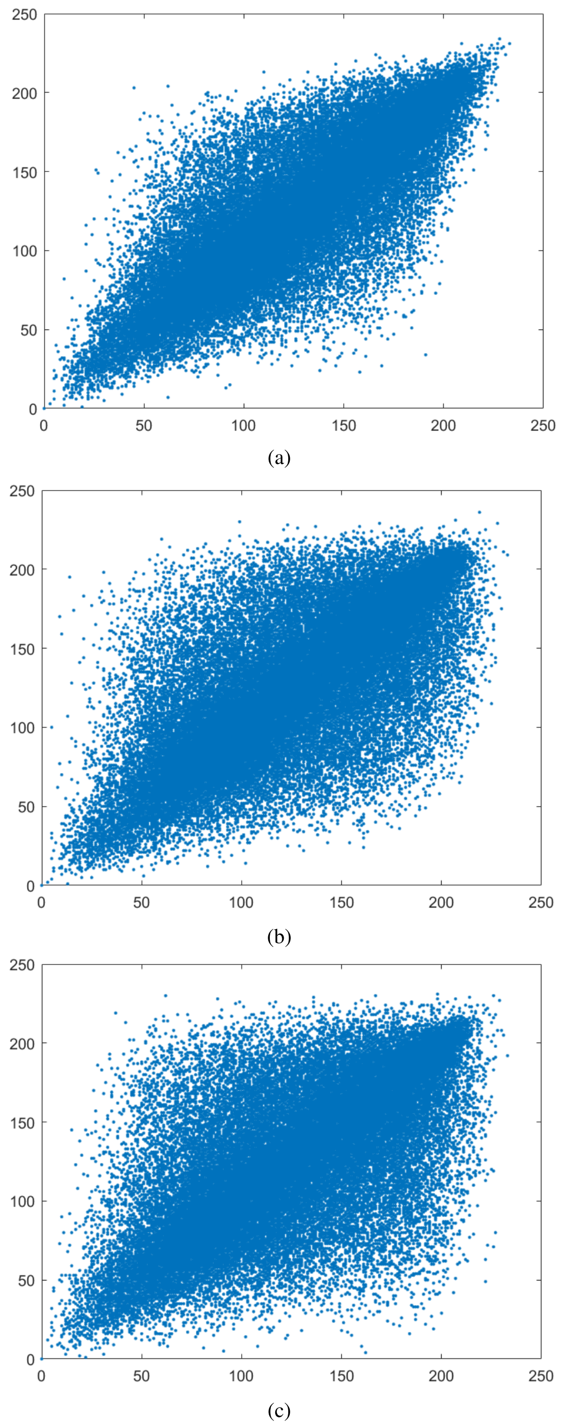

FIGURE 21. Correlation of neighborhood pixels at different directions of the plain image. (a) Horizontal directions. (b) Vertical directions. (c) Diagonal directions.

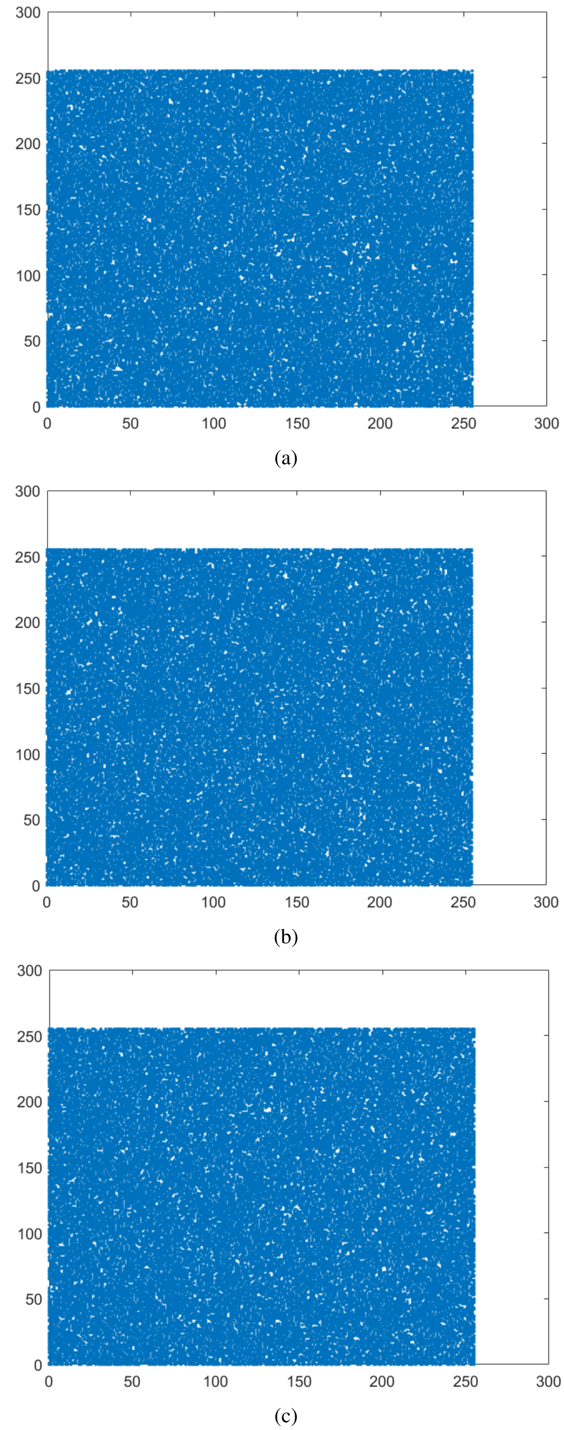

FIGURE 22. Correlation of neighborhood pixels at different directions of the encrypted image. (a) Horizontal directions. (b) Vertical directions. (c) Diagonal directions.

encrypted image shown in Fig. 16 are weak. It can also be illustrated by data in Table 1. Weak correlations and uniformly distributed histograms of the encrypted image indicate the application potential of finite-time projective synchronization of memristor-based BAM neural networks in image encryption and illustrate the effectiveness of Theorem 1.

Example 4: In this example, we use the simulation results from Example 2 to encrypt a new color plain image (as shown in Fig. 17). Processes of encryption and decryption are the same as those described in Example 3. Fig. 18 shows the encrypted image and its R, G, B components. Analysis of the encryption effect are exhibited in Fig. 19, Fig. 20,

TABLE 1. Correlation coefficients of adjacent pixel in the original image and in the encrypted image.

	Plain image	Encrypted image
horizontal direction	0.9906	-0.0071
vertical direction	0.9952	0.0004
diagonal direction	0.9915	-0.0012

TABLE 2. Correlation coefficients of adjacent pixel in the original image and in the encrypted image.

	Plain image	Encrypted image
horizontal direction	0.9587	0.0018
vertical direction	0.9652	-0.0006
diagonal direction	0.9791	-0.0008

Fig. 21 and Fig. 22. These figures and Table 2 indicate that the encrypted image has weak correlations and flat histograms, which means that the encryption algorithm can withstand statistical attack. The analysis of the experimental results show that the encryption algorithm is secure and practical. The potential application of MBAMNNs with stochastic perturbations and effectiveness of results obtained in Theorem 2 is verified.

V. CONCLUSION

In this paper, we have proposed two memristor-based BAM neural networks models with stochastic perturbations and time delays. These models have great chaotic properties, and then we applied them in our image encryption algorithm, respectively. To achieve the secure image transmission, some criteria have been obtained to guarantee the finite-time projective synchronization of drive-response system by constructing two feedback controllers. Encryption effect has demonstrated the security of our proposed image encryption algorithm and we have also analysed the potential applications of our models in secure image transmission.

REFERENCES

[1] H. Gao, Y. Zhang, S. Liang, and D. Li, "A new chaotic algorithm for image encryption," *Chaos, Solitons Fractals*, vol. 29, no. 2, pp. 393–399, Jul. 2006.

[2] L. Xu, Z. Li, J. Li, and W. Hua, "A novel bit-level image encryption algorithm based on chaotic maps," *Opt. Lasers Eng.*, vol. 78, pp. 17–25, Mar. 2016.

[3] H. S. Kwok and W. K. S. Tang, "A fast image encryption system based on chaotic maps with finite precision representation," *Chaos, Solitons Fractals*, vol. 32, no. 4, pp. 1518–1529, May 2007.

[4] B. Wang, F. C. Zou, and J. Cheng, "A memristor-based chaotic system and its application in image encryption," *Optik*, vol. 154, pp. 538–544, Feb. 2018.

[5] R. Matthews, "On the derivation of a 'chaotic' encryption algorithm," *Cryptologia*, vol. 8, no. 8, pp. 29–41, 1989.

[6] R. Parvaz and M. Zarebnia, "A combination chaotic system and application in color image encryption," *Opt. Laser Technol.*, vol. 101, pp. 30–41, May 2018.

[7] Y. Zhang, "A chaotic system based image encryption scheme with identical encryption and decryption algorithm," *Chin. J. Electron.*, vol. 26, no. 5, pp. 1022–1031, 2017.

[8] J. Gayathri and S. Subashini, "A spatiotemporal chaotic image encryption scheme based on self adaptive model and dynamic keystream fetching technique," *Multimedia Tools Appl.*, vol. 77, no. 19, pp. 24751–24787, 2018.

[9] Z. Hua and Y. Zhou, "Image encryption using 2D Logistic-adjusted-Sine map," *Inf. Sci.*, vol. 339, pp. 237–253, Apr. 2016.

[10] H. Natiq, N. M. G. Al-Saidi, M. R. M. Said, and A. Kilicman, "A new hyperchaotic map and its application for image encryption," *Eur. Phys. J. Plus*, vol. 133, no. 1, p. 6, Jan. 2018.

[11] B. Kosko, "Bidirectional associative memories," *IEEE Trans. Syst., Man, Cybern.*, vol. SMC-18, no. 1, pp. 49–60, Jan. 1988.

[12] K. Mathiyalagan, R. Sakthivel, and S. M. Anthoni, "New robust passivity criteria for stochastic fuzzy BAM neural networks with time-varying delays," *Commun. Nonlinear Sci. Numer. Simul.*, vol. 17, pp. 1392–1407, Mar. 2012.

[13] R. Sakthivel, R. Anbuvithya, K. Mathiyalagan, Y.-K. Ma, and P. Prakash, "Reliable anti-synchronization conditions for BAM memristive neural networks with different memductance functions," *Appl. Math. Comput.*, vol. 275, pp. 213–228, Feb. 2016.

[14] R. Anbuvithya, K. Mathiyalagan, R. Sakthivel, and P. Prakash, "Non-fragile synchronization of memristive BAM networks with random feedback gain fluctuations," *Commun. Nonlinear Sci. Numer. Simul.*, vol. 29, nos. 1–3, pp. 427–440, 2015.

[15] L. M. Pecora and T. L. Carroll, "Synchronization of chaotic systems," *Chaos Interdiscipl. J. Nonlinear Sci.*, vol. 25, no. 9, pp. 2891–5100, 2015.

[16] V. Milanovic and M. E. Zaghloul, "Synchronization of chaotic neural networks for secure communications," *Proc. ISCAS*, vol. 3, 1996, pp. 28–31.

[17] M. Yuan, X. Luo, W. Wang, L. Li, and H. Peng, "Pinning synchronization of coupled memristive recurrent neural networks with mixed time-varying delays and perturbations," *Neural Process. Lett.*, pp. 1–24, Mar. 2018.

[18] M. Yu, W. Wang, M. Yuan, X. Luo, and L. Liu, "Exponential anti-synchronization control of stochastic memristive neural networks with mixed time-varying delays based on novel delay-dependent or delay-independent adaptive controller," *Math. Problems Eng.*, vol. 2017, Mar. 2017, Art. no. 83147572.

[19] X. Li, C. Ding, and Q. Zhu, "Synchronization of stochastic perturbed chaotic neural networks with mixed delays," *J. Franklin Inst.*, vol. 347, no. 7, pp. 1266–1280, 2010.

[20] W. Wang, M. Yu, X. Luo, L. Liu, M. Yuan, and W. Zhao, "Synchronization of memristive BAM neural networks with leakage delay and additive time-varying delay components via sampled-data control," *Chaos Solitons Fractals*, vol. 104, pp. 84–97, Nov. 2017.

[21] W. Wang *et al.*, "Passivity of memristive BAM neural networks with leakage and additive time-varying delays," *Mod. Phys. Lett. B*, vol. 32, no. 4, p. 1850041, 2018.

[22] F. Rihan, C. Rajivganthi, S. Lakshmanan, R. Rakkiyappan, and P. Muthukumar, "Synchronization of memristor-based delayed BAM neural networks with fractional-order derivatives," *Complexity*, vol. 21, no. S2, pp. 412–426, 2016.

[23] W. Wang, M. Yuan, X. Luo, L. Liu, and Y. Zhang, "Anti-synchronization control of bam memristive neural networks with multiple proportional delays and stochastic perturbations," *Mod. Phys. Lett. B*, vol. 32, no. 3, p. 1850028, 2018.

[24] J. Xiao, S. Zhong, Y. Li, and F. Xu, "Finite-time Mittag-Leffler synchronization of fractional-order memristive BAM neural networks with time delays," *Neurocomputing*, vol. 219, pp. 431–439, Jan. 2016.

[25] G. Velmurugan, R. Rakkiyappan, and J. D. Cao, "Finite-time synchronization of fractional-order memristor-based neural networks with time delays," *Neural Netw.*, vol. 73, pp. 36–46, Jan. 2016.

[26] M. Jiang, S. Wang, J. Mei, and Y. Shen, "Finite-time synchronization control of a class of memristor-based recurrent neural networks," *Neural Netw.*, vol. 63, pp. 133–140, Mar. 2014.

[27] H. Wu, X. Zhang, R. Li, and R. Yao, "Finite-time synchronization of chaotic neural networks with mixed time-varying delays and stochastic disturbance," *Memetic Comput.*, vol. 7, no. 3, pp. 231–240, 2015.

[28] W. Wang, L. Li, P. Haipeng, J. Kurths, J. Xiao, and Y. Yang, "Finite-time anti-synchronization control of memristive neural networks with stochastic perturbations," *Process. Lett.*, vol. 43, no. 1, pp. 49–63, 2014.

[29] Y. Shi and P. Zhu, "Finite-time synchronization of stochastic memristor-based delayed neural networks," *Neural Comput. Appl.*, vol. 29, no. 6, pp. 293–301, 2016.

[30] K. Z. Li, M. C. Zhao, and X. C. Fu, "Projective synchronization of driving-response systems and its application to secure communication," *IEEE Trans. Circuits Syst. I, Reg. Papers*, vol. 56, no. 10, pp. 2280–2291, Oct. 2009.

[31] H. Liu, Z. Zhu, H. Yu, and Q. Zhu, "Modified projective synchronization between different fractional-order systems based on open-plus-closed-loop control and its application in image encryption," *Math. Problems Eng.*, vol. 2014, Mar. 2014, Art. no. 567898.

[32] Z. Li and D. Xu, "A secure communication scheme using projective chaos synchronization," *Chaos, Solitons Fractals*, vol. 22, no. 2, pp. 477–481, 2004.

[33] H.-B. Bao and J.-D. Cao, "Projective synchronization of fractional-order memristor-based neural networks," *Neural Netw.*, vol. 63, pp. 1–9, Mar. 2015.

[34] H. Wu, R. Li, R. Yao, and X. Zhang, "Weak, modified and function projective synchronization of chaotic memristive neural networks with time delays," *Neurocomputing*, vol. 149, pp. 667–676, Feb. 2015.

[35] R. Li, H. Wu, X. Zhang, and H. Wu, "Adaptive projective synchronization of memristive neural networks with time-varying delays and stochastic perturbation," *Math. Control Related Fields*, vol. 5, no. 4, pp. 827–844, 2015.

[36] F. Wang, W. Zhou, and Y. Ran, "A class of delayed BAM self-adaptive neural network with uncertain parameters for projective synchronization problem," in *Proc. 7th Int. Conf. Natural Comput.*, 2011, pp. 481–485.

[37] C. Chen, L. Li, H. Peng, and Y. Yang, "Fixed-time synchronization of memristor-based BAM neural networks with time-varying discrete delay," *Neural Netw.*, vol. 96, pp. 47–54, Dec. 2017.

[38] X. Mao, "A note on the LaSalle-type theorems for stochastic differential delay equations," *J. Math. Anal. Appl.*, vol. 268, no. 1, pp. 125–142, 2002.

[39] G. H. Hardy and J. E. Littlewoodwrited, *Inequalities*. 1952.

[40] Y. Tang, "Terminal sliding mode control for rigid robots," *Automatica*, vol. 34, no. 1, pp. 51–56, 1998.

WEIPING WANG received the Ph.D. degree in telecommunications physics electronics from the Beijing University of Posts and Telecommunications, Beijing, China, in 2015. She is currently an Associate Professor with the Department of Computer and Communication Engineering, University of Science and Technology Beijing. Her current research interests include brain-like computing, memrisitive neural network, associative memory awareness simulation, complex network, network security, and image encryption. She received the National Natural Science Foundation of China, the post-doctoral fund, and the basic scientific research project.

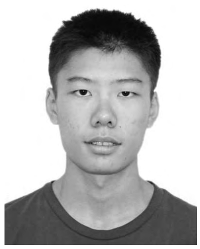

XIAO WANG is currently pursuing the bachelor's degree in information security with the University of Science and Technology Beijing, Beijing, China. His current research interests include memristor-based neural networks, data compression, and image encryption.

XIONG LUO (M'16) received the Ph.D. degree in computer applied technology from Central South University, Changsha, China, in 2004. He is currently a Professor with the School of Computer and Communication Engineering, University of Science and Technology Beijing, Beijing, China. His current research interests include neural networks, machine learning, and computational intelligence. He has published extensively in his areas of interest in several journals, such as the IEEE Access, *Future Generation Computer Systems*, and *Personal and Ubiquitous Computing*.

MANMAN YUAN received the M.S. degree in computer science and technology from the Inner Mongolia University of Science and Technology, Baotou, China, in 2015. She is currently pursuing the Ph.D. degree from the University of Science and Technology Beijing, Beijing, China. Her current research interests include memristive neural networks and brain computing.